

KrkNLO matching and phenomenology for vector boson processes

Pratixan Sarmah,^a Andrzej Siódmok,^{a,b} James Whitehead^a

^a*Jagiellonian University,
ul. prof. Stanisława Łojasiewicza 11, 30-348 Kraków, Poland*

^b*Theoretical Physics Department, CERN,
1211 Geneva 23, Switzerland*

E-mail: pratixan.sarmah@doctoral.uj.edu.pl, andrzej.siodmok@uj.edu.pl,
james.whitehead@uj.edu.pl

ABSTRACT: The combination of NLO matrix elements with parton showers is indispensable for LHC physics. Differences between matching methods introduce matching uncertainties, corresponding to formally higher-order terms. We recently presented the process-independent generalisation of the KrkNLO method for NLO matching, which employs a modified PDF factorisation scheme to achieve NLO accuracy. With this factorisation scheme, the method can be used for colour-singlet final-states, and was previously implemented in the `Herwig` Monte Carlo Event Generator and applied to the diphoton-production process.

Here we present the extension of the implementation of the KrkNLO method within `Herwig` to support the full class of applicable processes, using an external matrix-element library. We re-validate the implementation, and use it to study the NLO matching uncertainty for four vector-boson production processes at the LHC: W , $Z\gamma$, WW and ZZ . We demonstrate that the KrkNLO method effectively eliminates the negative-weight problem in NLO event generation, across the four processes studied. We provide detailed comparisons between KrkNLO and variants of the `Mc@NLO` method with different shower starting-scale choices, across processes and throughout phase-space, including double-differential observables. For each process, we compare the predictions to LHC data from ATLAS.

KEYWORDS: QCD, LHC, NLO matching, parton showers, hadron colliders

Contents

1	Introduction	1
2	The KrkNLO method	2
3	Validation	3
3.1	Real validation	3
3.2	Virtual validation	3
3.3	Non-diagonal CKM matrix	3
4	Analysis of NLO matching uncertainty	6
4.1	First-emission only	8
4.2	Full shower	13
5	LHC phenomenology	18
5.1	Charged-current Drell–Yan	18
5.2	$Z\gamma$ production	18
5.3	WW production	20
5.4	ZZ production	20
6	Conclusions	23
A	Positivity of KrkNLO event-weights	25
B	Unabridged double-differential distributions	25

1 Introduction

‘Matched’ calculations combining next-to-leading-order (NLO) perturbative accuracy with the logarithmic resummation of parton shower algorithms remain indispensable for LHC phenomenology. Two methods for matching at NLO, the `MC@NLO` [1] and `POWHEG` methods [2–4], have been widely used for LHC physics.¹ The matching uncertainties associated with these methods have been investigated for a number of processes and independent implementations in [14–26].

The differences between results generated by alternative matching schemes may be considered ‘matching uncertainties’, and correspond to formally higher-order terms introduced beyond NLO by the choice of matching method. The presence of logarithms of ratios of scales, generated by the evolution of the parton shower, allows such uncertainties to be numerically larger than their formal perturbative suppression would naively suggest.

In [27] we recapitulated the KrkNLO method [28–30], generalised to the production of arbitrary colour-singlet final-states which proceed via $q\bar{q}$ -annihilation at leading-order, and outlined its implementation in `Herwig 7` [31, 32].² The KrkNLO method uses the freedom, at NLO and beyond, to choose a factorisation scheme for the parton distribution functions (PDFs). The scheme used,

¹A number of others, at NLO and beyond, have been proposed or are in development or use [5–13].

²For convenience, in this work we adopt the notation and conventions of [27], which may be considered a companion paper to this one.

the Krk scheme [33], simplifies the matching calculation by moving collinear counterterms from the hard process into the PDFs. We used diphoton production as a test process, with hard-coded real-emission and virtual matrix elements. This was the first process calculated with the KrkNLO method that was not used for the definition of the Krk factorisation scheme.

In this work, we report on the extension of the KrkNLO code to support arbitrary processes calculable by the KrkNLO method, using the `OpenLoops` library [34] to compute the matrix-elements. This enables the KrkNLO method to be applied to the full class of suitable processes. Here, we focus on four processes involving the production of at least one massive vector-boson: $pp \rightarrow \{W, Z\gamma, WW, ZZ\}$.³ With this we demonstrate the full breadth of applicability of the method, and the computational readiness of the code.

For each included process, we follow the general strategy applied to diphoton-production in [27]: we (i) demonstrate the numerical validation of the KrkNLO implementation, in section 3; (ii) perform a theory comparison to fixed-order NLO and MC@NLO, both with the parton shower truncated to a single emission, and running to completion, in section 4, and (iii) examine the resulting phenomenology using experimental data from the LHC, in section 5. We find that the KrkNLO method gives the expected level of agreement with the LHC data for an NLO calculation, and that the KrkNLO prediction is not necessarily within the matching-uncertainty envelope obtained by shower starting-scale variation within the MC@NLO method.

2 The KrkNLO method

The KrkNLO method generates events from the Born m -particle phase-space Φ_m , and uses the shower algorithm itself to generate events with real-emission kinematics Φ_{m+1} . According to the decision tree implied by the shower algorithm, events are reweighted multiplicatively to incorporate the real and virtual matrix-elements, R and V , in a way that leads to positive event-weights subject to the positivity of the PDFs and the virtual reweight. By avoiding subtraction, the method eliminated a common source of negative weights in the MC@NLO method.⁴

The method may be summarised succinctly as:

```

for all Born events do shower
  if first emission generated, from kernel ( $\alpha$ ) then
     $w \leftarrow w \times \frac{R(\Phi_{m+1})}{P_m^{(\alpha)}(\Phi_{m+1}) B(\Phi_m)}$ 
  end if
   $w \leftarrow w \times \left[ 1 + \frac{\alpha_s(\mu_R)}{2\pi} \left( \frac{V(\Phi_m; \mu_R)}{B(\Phi_m)} + \frac{I(\Phi_m; \mu_R)}{B(\Phi_m)} + \Delta_0^{\text{FS}} \right) \right]$ 
end for

```

Here $P_m^{(\alpha)}$ denotes the splitting function that generated the selected splitting within the shower algorithm; I , the contribution from the Catani **I**-operator, corresponding here to integrated Catani–Seymour dipoles; μ_R , the renormalisation scale, and Δ_0^{FS} a factorisation-scheme-dependent constant which corrects for endpoint-contributions absorbed into the PDFs.

When combined with the use of PDFs in the Krk factorisation scheme [33, 35], no further collinear convolutions are required, allowing the NLO matching condition to be satisfied through multiplicative reweighting alone.

A full exposition, including formulae for the resulting contributions to a given IR-safe observable \mathcal{O} , is given in [27].

³In [29] the KrkNLO method was applied to neutral-current Drell–Yan production in an approximation factorising Z -boson production from its decay. In this work we use exact matrix-elements, unapproximated.

⁴Positivity is discussed further in section A.

3 Validation

In this section we apply the validation strategy introduced for the diphoton process in [27], illustrating the validation of the KrkNLO code for each of the processes considered in this study. This also documents the validation of the `OpenLoops` KrkNLO implementation that will be made publicly available as part of `Herwig` 7.4. These tests are performed with generation parameters and analysis cuts (via `Rivet` [36]) as used in section 4, except where stated otherwise.

3.1 Real validation

As in [27], we test the reweight implementing the real-emission correction by truncating the parton shower after one-emission, and vetoing the no-emission contributions; the Sudakov factor generated by the veto algorithm within the parton shower is calculated numerically, and its reciprocal applied as a reweight.

Since the one-emission truncation of the shower algorithm changes the result only at $\mathcal{O}(\alpha_s^2)$, and the Sudakov factor (and its reciprocal) are formally 1 to leading-order, this provides numerical verification that the method achieves NLO-accuracy in this region of phase-space.

The resulting differential cross-sections are shown in fig. 1, compared against those arising from the real-emission matrix-element, i.e. the sole contribution to $\mathcal{O}(\Phi_{m+1})$ within an NLO calculation of $pp \rightarrow X$ (equivalently, within a leading-order calculation of $pp \rightarrow X + j$), calculated with `Matchbox` [18] within `Herwig` 7.

We show both the symmetrised and unsymmetrised versions of KrkNLO as presented in [27].⁵ We see agreement to the percent level for the symmetrised version. For the unsymmetrised KrkNLO variant, agreement is at the few-percent level and within statistical uncertainties, limited by slower statistical convergence (due to large weights, some visible) and fewer generated events.

3.2 Virtual validation

As in [27], we isolate the implementation of the virtual reweight within the KrkNLO code by setting the parton shower cutoff scale sufficiently high to prohibit any parton-shower radiation. The radiative phase-space is then empty, and as a consequence the Sudakov factor representing the no-emission probability is identically 1. To isolate the one-loop matrix-element contribution V and Catani–Seymour I-operator terms within the virtual reweight, we disable the Born and Δ_0^{Krk} terms (setting them to zero within the code).

The resulting differential cross-sections are shown in fig. 2, compared against those computed using the corresponding automated `Matchbox` implementation within `Herwig`, calculated with one-loop matrix-elements provided by either `MadGraph` or `OpenLoops` as shown. We see percent-level agreement in general, and permille-level wherever the statistical convergence is sufficient to resolve this level of precision.

3.3 Non-diagonal CKM matrix

The validation plots presented above were calculated using the flavour-diagonal identity-matrix approximation for the Cabibbo–Kobayashi–Maskawa (CKM) mixing matrix, which is used by default within `Matchbox`. For processes involving W -bosons the effect of the true CKM is not guaranteed to be negligible. In fig. 3 we therefore present the validation of the KrkNLO code in the case of W -production for the full, non-diagonal, CKM mixing matrix, using the `Herwig` defaults (taken

⁵The symmetrised real weight averages over the two possible underlying Born phase-space configurations for each real-emission configuration, rather than only using the Born phase-space point actually generated as the initial condition for the shower, in order to regulate the real-reweight distribution. As outlined in [27], we consider the symmetrised version to be the default, and use it for the remainder of this work.

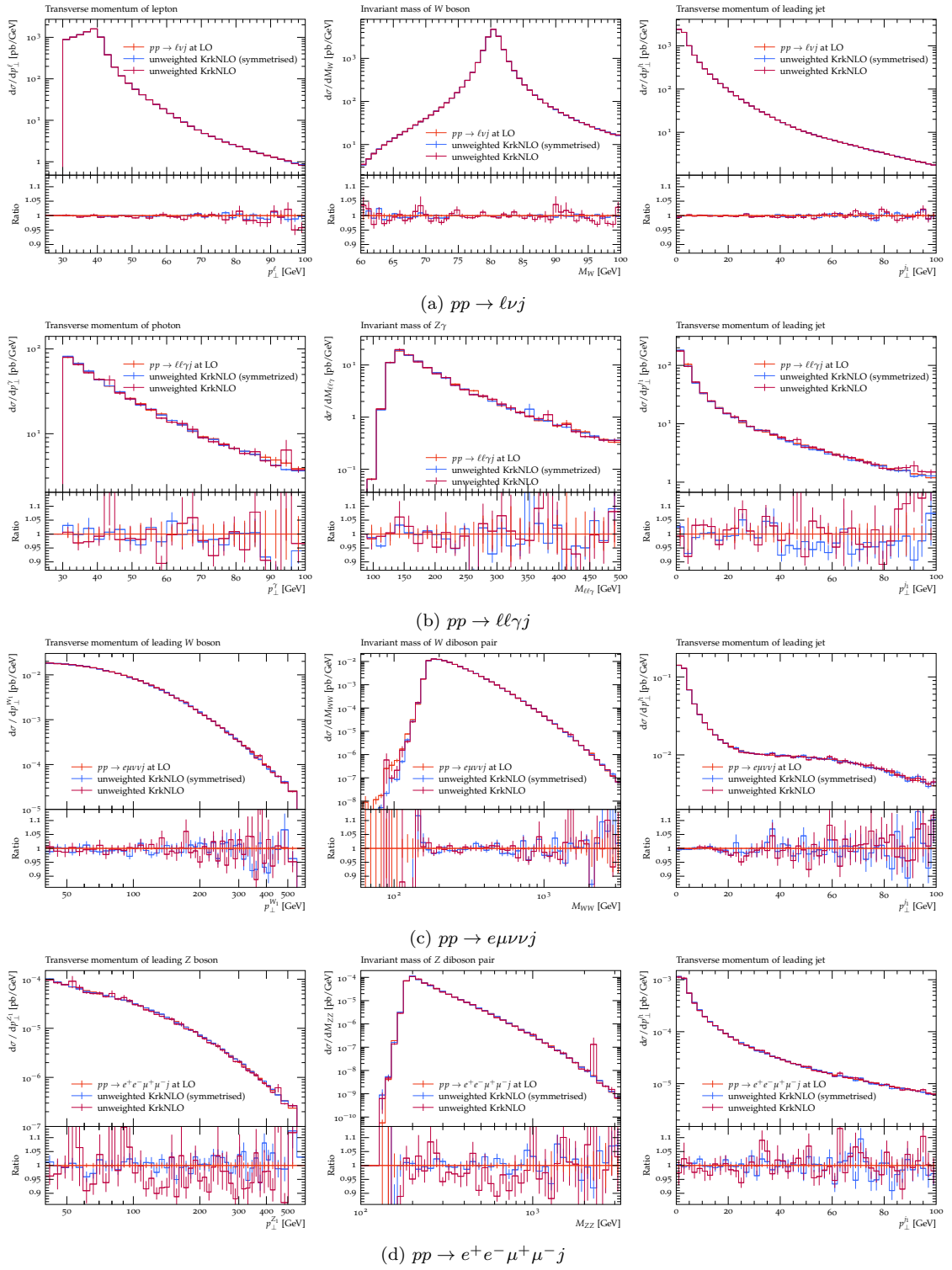


Figure 1: Validation of the real weight, unweighting by the first-emission Sudakov factor $\Delta|_{p_{T,1}}^{Q(\Phi_m)}(\Phi_m)$ (independently calculated for each emission by numerical integration of the kernels over the radiative phase-space) to isolate the real matrix element within the KrkNLO implementation. Plots shown for the W , $Z\gamma$, WW , and ZZ processes respectively.

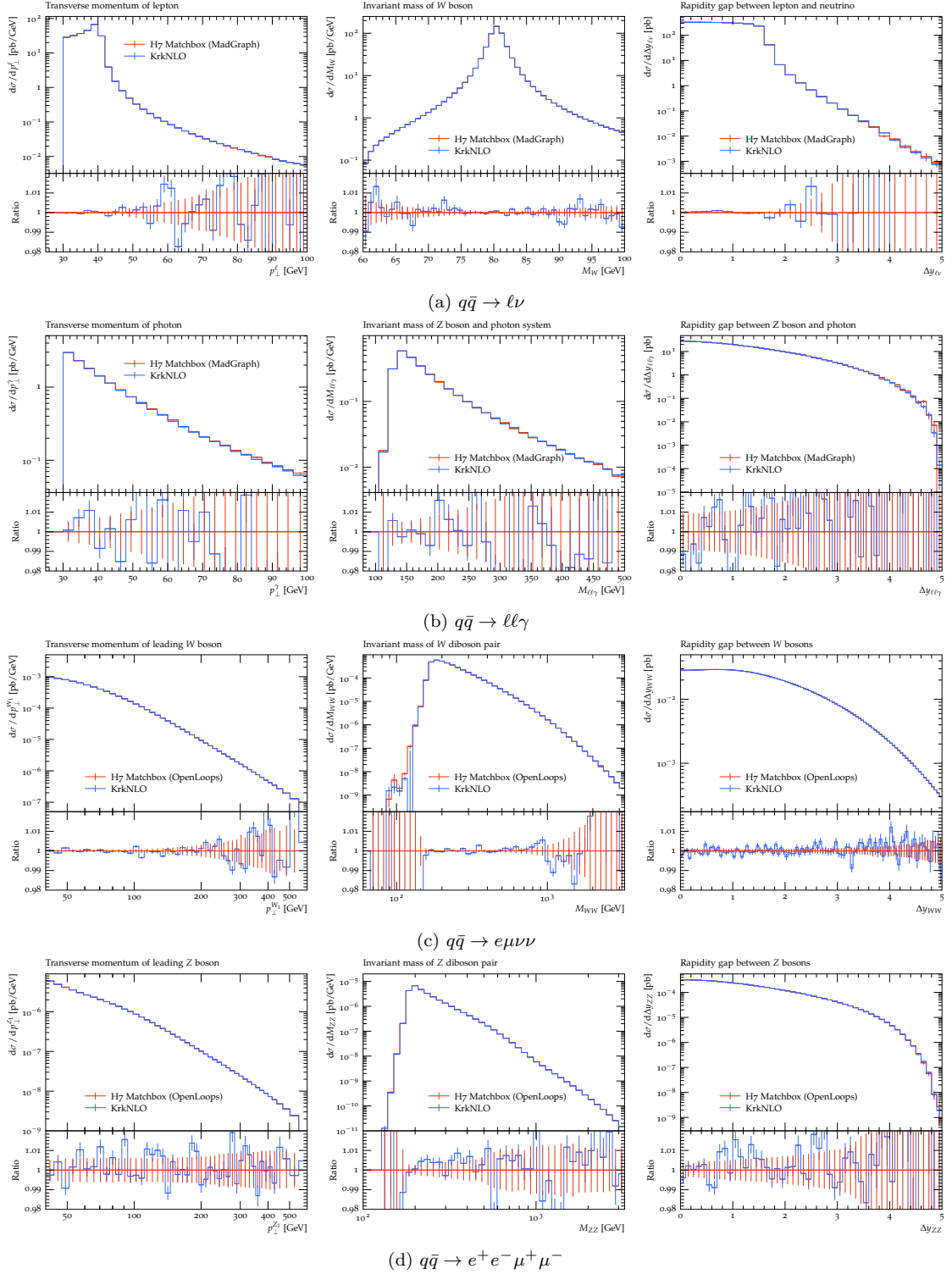


Figure 2: Validation of the virtual weight $V + I$ for the $q\bar{q}$ -channel as described in [27]. By setting the shower IR cutoff to guarantee $t_0 > Q(\Phi_m)$, thus disabling the shower, and manually disabling the Born and Δ_0^{Krk} contributions within KrkNLO, the KrkNLO implementation of the virtual terms can be isolated and compared with those generated automatically by Matchbox within Herwig 7. Plots shown for the W , $Z\gamma$, WW and ZZ processes respectively.

from the PDG [37]) for both the KrkNLO calculation and the `Matchbox` reference.⁶ Within the KrkNLO implementation, the CKM matrix elements set within `Herwig` are automatically passed to `OpenLoops`, and may therefore be changed using the usual interface.

4 Analysis of NLO matching uncertainty

In general, we follow the same approach as for diphoton production in [27], to allow a systematic comparison of matching methods and the associated matching uncertainties, across the processes.

We use `Herwig 7` for all predictions, and the `Herwig 7` implementation [38] of the dipole shower [39–42], based on the Catani–Seymour subtraction formalism [43]. Within the KrkNLO method, the choice of factorisation scale is determined by the NLO matching condition.⁷ We therefore consistently adopt the renormalisation and factorisation scales

$$\mu_R(\Phi_m) = \sqrt{\hat{s}_{12}} \equiv M = \mu_F(\Phi_m) \quad (4.1)$$

$$\mu_R(\Phi_{m+1}) = M = \mu_F(\Phi_{m+1}), \quad (4.2)$$

for KrkNLO, `Mc@NLO` and the fixed-order NLO calculations, where M is the invariant mass of the m -particle colourless final state system which defines the process at leading-order, and Φ_m is the m -particle Born phase-space (and Φ_{m+1} the real-emission phase-space).⁸

Within the parton shower we use the scale $\mu^{(\alpha)} = \|\mathbf{k}_T^{(\alpha)}\|$, the transverse-momentum of the generated splitting relative to the emitter-spectator dipole, for both the ratios of PDFs and for the running of α_s .

For `Mc@NLO` we consider several comparators with alternative choices of shower starting scale:

- a ‘power-shower’ with $Q(\Phi_m) = Q_{\max}(\Phi_m)$ and $Q(\Phi_{m+1}) = Q_{\max}(\Phi_{m+1})$;⁹
- a ‘default’ shower with $Q(\Phi_m) = \sqrt{\hat{s}_{12}} \equiv M$ and $Q(\Phi_{m+1}) = p_T^{j_1}$;
- a ‘DGLAP-inspired’ choice in which the shower starting-scale consistently matches the factorisation scale, here $Q(\Phi_m) = M$ and $Q(\Phi_{m+1}) = M$.

For the KrkNLO method, the shower starting-scale is fixed to $Q_{\max}(\Phi_m)$, namely the largest scale kinematically-accessible from the Born phase-space, which is required to populate the full real-emission phase-space and thus to satisfy the NLO matching condition.⁷

Throughout we use `CT18NLO` PDFs [45], either in the $\overline{\text{MS}}$ scheme or transformed into the Krk scheme as described in [27]. Accordingly, we adopt $\alpha_s(M_Z) = 0.118$ as the input to the running of the strong coupling throughout the hard process, shower, and the KrkNLO code. We use loose generator cuts, summarised in table 1, to avoid excluding regions of phase-space that would contribute to the fiducial region after showering. We use the `Herwig 7` default dipole-shower cutoff scale $p_T^{\text{cut}} = 1 \text{ GeV}$. Within `Herwig` we disable both hadronisation and the `RemnantDecayer`, so the final-state of the hard-process is the only source of final-state QCD partons, and the hard-process is the only input into the parton shower initial-conditions.

⁶Note that for the runs presented in sections 4 and 5, the default diagonal approximation has been used.

⁷See [27] for details of the NLO matching condition and the KrkNLO method.

⁸To avoid cluttering the plots, we do not consider scale-variations, which like matching-uncertainty is formally-NNLO. Indicative estimates for the scale-uncertainty of the processes considered here are available in the literature cited for each process.

⁹Note that the ‘power-shower’ choice for `Mc@NLO` is generally not recommended [44], and is included to enable a direct comparison with the power-shower choice required by KrkNLO. For `Mc@NLO`, the power-shower provides a strict upper-bound for the shower starting-scale and so corresponds to one edge of the uncertainty envelope.

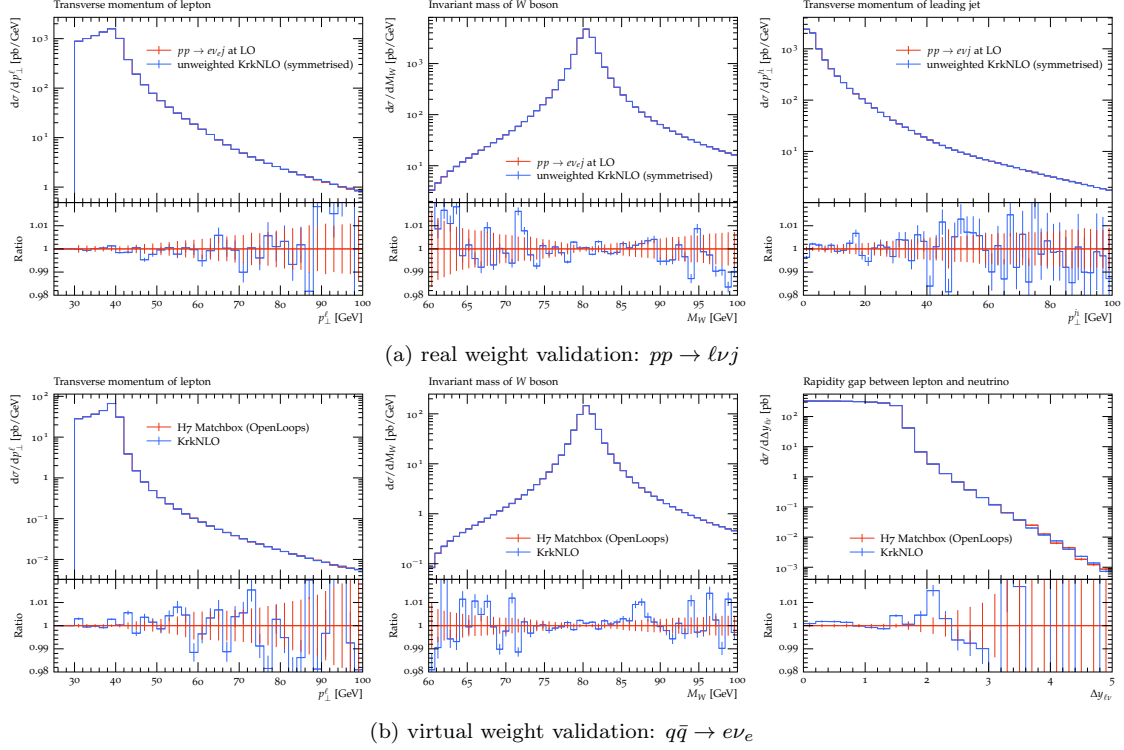


Figure 3: Validation of the KrkNLO implementation using a non-diagonal CKM matrix, for the process $pp \rightarrow W \rightarrow \ell\nu$. This figure is a counterpart to figs. 1a and 2a, which are identical save that the CKM matrix is there approximated by the identity matrix.

In contrast with the results for the diphoton process studied in [27], in this work we do not include the gg -channel loop-induced diagrams (formally NNLO).¹⁰ For each process we state the approximate magnitude of the missing NNLO corrections in section 5.

In this section we perform a systematic comparison of the matching schemes under consideration, between KrkNLO and the three variants of MC@NLO outlined in section 4 ('power-shower', 'default', and 'DGLAP'). We make two comparisons between matching schemes, which we label 'first-emission' and 'full-shower', in section 4.1 and section 4.2 respectively.

For 'first-emission' comparisons, we consistently truncate the shower in the Φ_{m+1} phase-space. For MC@NLO, this corresponds to 'H'-events with no shower emissions, and 'S'-events with at most one shower emission. At this point, the matching between the hard-process and the shower is complete, and the subsequent evolution of each event is handled entirely by the parton shower algorithm, which is the same in both cases.¹¹ In the case of the KrkNLO method, the soft-virtual reweight is not applied to the one-emission events.

For 'full-shower' comparisons, we allow the shower to run to its final cutoff scale, fully populating the multiple-emission phase-space. This gives the full matched prediction, which we further use to perform the comparisons with experimental data from the LHC in section 5.

We use generator cuts as given in table 1 and apply analysis cuts as summarised in table 2. These have been chosen to give acceptance regions with similar kinematics across the different

¹⁰These may be expected to make a difference to the overall level of numerical agreement with experimental data, but not to the differences between the alternative matching schemes.

¹¹This is subject to the caveat that the shower starting-scale for the first 'post-matching' emission, $Q(\Phi_{m+1})$ within MC@NLO, may not match the starting-scale for the second-emission continuation of the shower within KrkNLO.

Process	Centre-of-mass energy \sqrt{s}	Generation cuts
$pp \rightarrow W \rightarrow \ell\nu$	7 TeV	$p_T^{\ell,\nu} > \begin{cases} 15 \text{ GeV} & \text{Mc@NLO} \\ 1 \text{ GeV} & \text{KrkNLO} \\ M_{\ell\nu} > 45 \text{ GeV} \end{cases}$
$pp \rightarrow Z\gamma \rightarrow \ell\ell\gamma$	13 TeV	$p_T^\ell > \begin{cases} 5 \text{ GeV} & \text{Mc@NLO} \\ 5 \text{ GeV} & \text{KrkNLO} \end{cases}$ $p_T^\gamma > \begin{cases} 10 \text{ GeV} & \text{Mc@NLO} \\ 5 \text{ GeV} & \text{KrkNLO} \end{cases}$ $M_{\ell\ell} > 35 \text{ GeV}$
$pp \rightarrow WW \rightarrow e\mu\nu_e\nu_\mu$	13 TeV	$p_T^{\ell,\nu} > 1 \text{ GeV},$ $ y^{\ell,\nu} < 25$
$pp \rightarrow ZZ \rightarrow \ell\ell\ell\ell$	13 TeV	$p_T^{\ell,\nu} > 1 \text{ GeV},$ $ y^{\ell,\nu} < 25$

Table 1: Energy scale and generation cuts applied for each process.

processes. For the $Z\gamma$ process, in place of experimental photon isolation we use smooth-cone ('Frixione') isolation [46] with the 'tight' isolation parameters from the 2013 Les Houches Accords [47], which corresponds to

$$\chi(r; R) = \left(\frac{1 - \cos r}{1 - \cos R} \right) \equiv \left(\frac{\sin \frac{1}{2}r}{\sin \frac{1}{2}R} \right)^2, \quad (4.3)$$

where $E_T^{\text{iso}}(r)$ is the cumulative transverse isolation energy within (rapidity-azimuth) radius r , calculated as the transverse magnitude of the total momentum of all non-photon particles within a cone of radius r .

Where jet distributions are shown, jets are identified using the anti- k_T algorithm [48] with a jet clustering radius of 0.4, a p_T -cut of 1 GeV and a pseudo-rapidity cut $|\eta| < 4.5$.

4.1 First-emission only

Differential cross-sections for the invariant mass of the colour-singlet system, and the azimuthal angle and rapidity separation between the constituents of the colour-singlet system (the two bosons for diboson processes; lepton and neutrino for W) are shown in fig. 4. These observables have been chosen to characterise the imputed underlying two-particle final-state of the Born-level $2 \rightarrow 2$ hard-process, prior to subsequent boson decay or additional QCD radiation.

Differential cross-sections for the transverse momentum and the rapidity of the leading jet are shown in fig. 5. To clarify the roles of the QCD radiation and corresponding Sudakov factors across phase-space, differential cross-sections for the invariant mass of the colour-singlet system in slices of the transverse momentum of the leading jet are shown in fig. 6.¹³

¹²For the results presented in this section, we avoid issues related to the possible ambiguity of ZZ -reconstruction by restricting only to final-states containing different-flavour lepton-pairs.

¹³Throughout we will refer to such distributions as 'double-differential'; note, however, that for ease of comparability between figures, they have not been normalised to the bin-width of the second observable. They are therefore single-differential distributions, 'in slices of' the second observable.

Process	Analysis cuts
$pp \rightarrow W \rightarrow \ell\nu$	$p_T^\ell > 30 \text{ GeV}$, $p_T^\nu > 25 \text{ GeV}$ $ y^{\ell,\nu} < 5$ $M_{\ell\nu} > 50 \text{ GeV}$
$pp \rightarrow Z\gamma \rightarrow \ell\ell\gamma$	$p_T^{\ell_1} > 30 \text{ GeV}$, $p_T^{\ell_2} > 25 \text{ GeV}$, $p_T^\gamma > 30 \text{ GeV}$ $ y^{\ell,\gamma} < 2.5$ $M_{\ell\ell} > 40 \text{ GeV}$ $\Delta R_{\ell\gamma} > 0.4$ $E_T^{\text{iso}}(r) < 0.1 p_T^\gamma \chi(r; R)$ within cone $r \leq R = 0.2$
$pp \rightarrow WW \rightarrow e\mu\nu_e\nu_\mu$	$p_T^\ell > 30 \text{ GeV}$, $ y^\ell < 2.5$ $p_T^{\text{miss}} > 20 \text{ GeV}$ $M_{\ell\nu} \in [60, 100] \text{ GeV}$
$pp \rightarrow ZZ \rightarrow e^+e^-\mu^+\mu^-$ ¹²	$p_T^\ell > 30 \text{ GeV}$ $ y^\ell < 2.5$ $M_{\ell\ell} \in [65, 115] \text{ GeV}$

Table 2: Summary of fiducial cuts applied for each process for the matching study in section 4. The boson reconstruction from the leptonic final-state is performed at truth-level.

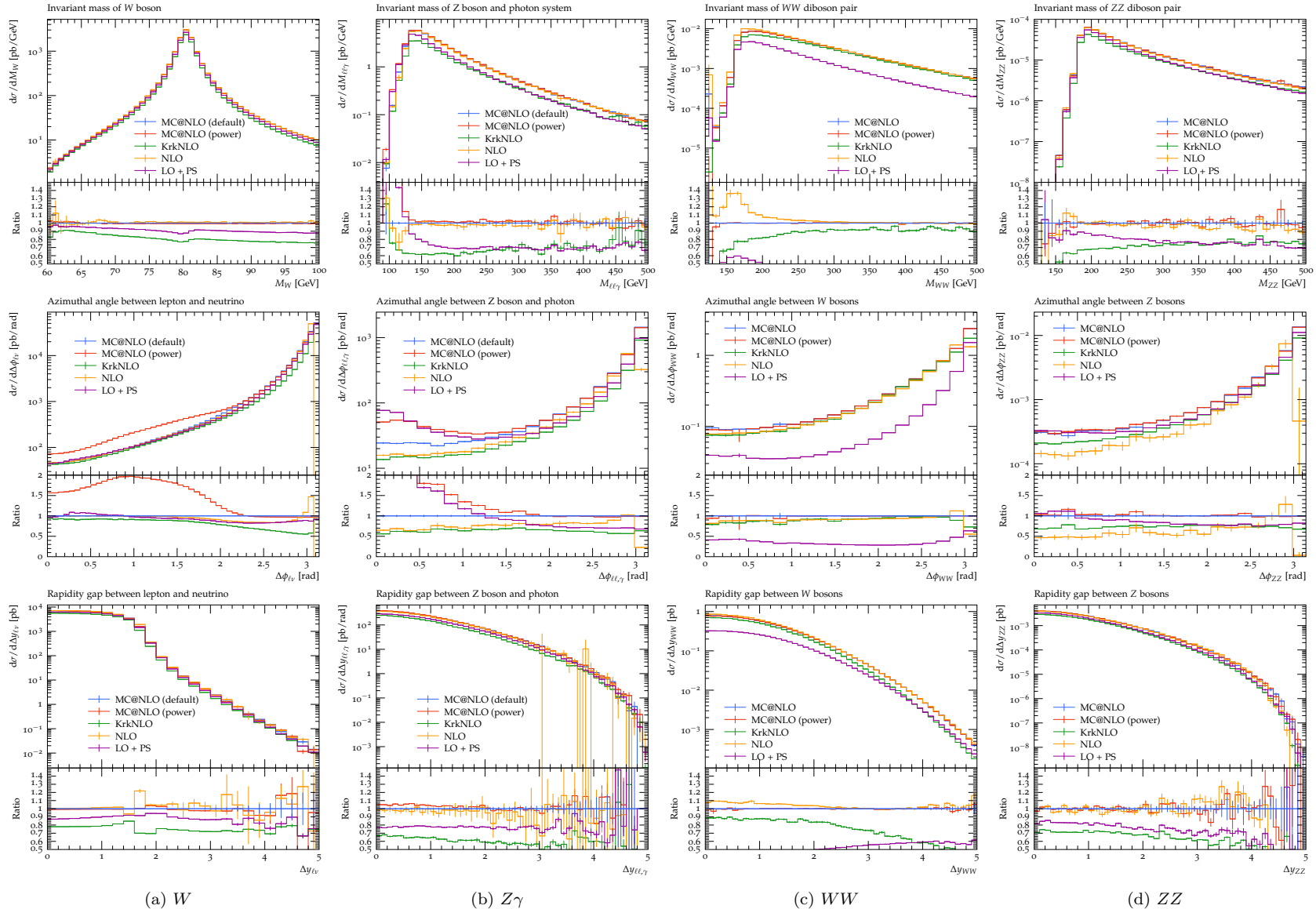


Figure 4: ‘Parton level’ (first-emission) comparison of KrkNLO with MC@NLO, NLO fixed-order, and the corresponding first-emission distributions generated by the parton shower from a leading-order calculation.

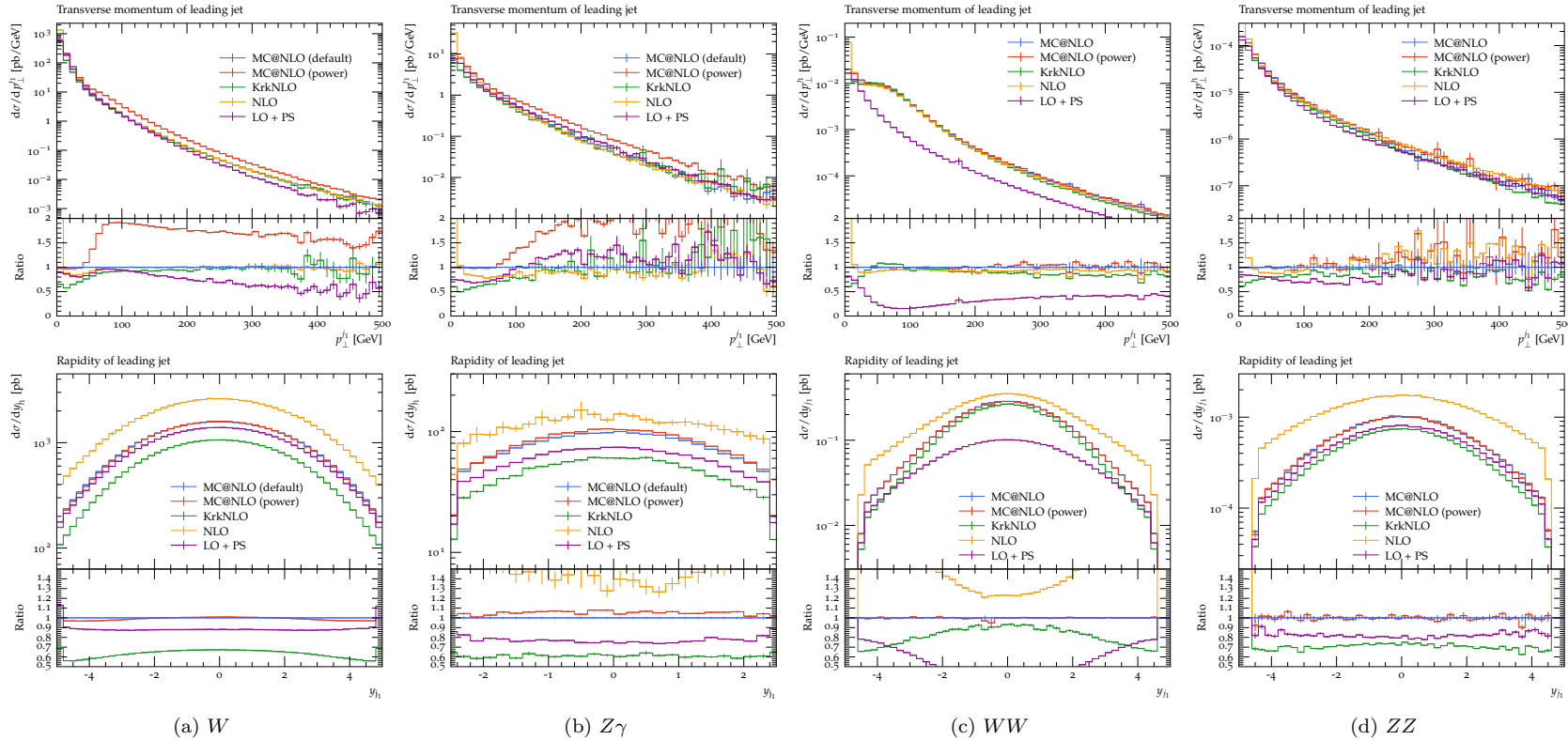


Figure 5: ‘Parton level’ (first-emission) comparison of the QCD radiation arising from KrkNLO with MC@NLO, NLO fixed-order, and the first-emission generated by the parton shower from a leading-order calculation. Note that here, due to the multiplicity of the final-state, there is at most one jet, and it comprises a single parton.

The transverse momentum of the leading jet, shown in fig. 5, is consistently-described at high- p_T between fixed-order NLO, the KrkNLO method and MC@NLO (default). This is largely as expected, due to the role of the real-emission matrix-element in providing (leading-order) perturbative accuracy in this region. For processes with a massless particle in the $2 \rightarrow 2$ final-state, the matching uncertainty within the MC@NLO method due to the choice of shower starting-scale is significant.¹⁴ From the double-differential plots of fig. 6, we see that the agreement in this high- p_T region is also reached double-differentially in invariant mass, save for $Z\gamma$ which deviates only for the MC@NLO power-shower prediction (which agrees with the showered leading-order prediction) at low- M .

At low- p_T^j , the Sudakov factor $\Delta|_{p_T^{j_1}}^{Q(\Phi_m)}(\Phi_m)$ can be seen in figs. 5 and 6 to tame the characteristic divergence of the real-emission matrix element in all cases. This is the limit in which perturbation theory breaks down and the all-order resummation provided by the shower (here, truncated to a single emission) becomes relevant. The variants of MC@NLO converge here, due to the low sensitivity of emissions at this low scale to the upper-limit of shower-radiation, and as a result the KrkNLO prediction lies outwith the implied MC@NLO matching-uncertainty envelope. This suppression dominates the overall differences seen in the inclusive distributions, as shown in further detail in fig. 7 and discussed below. Note that the magnitude of the suppression induced by the Sudakov factor is a function of the choice of shower cutoff-scale p_T^{cut} , here set to 1 GeV. The difference between the KrkNLO and leading-order predictions in this region is attributable to the use of the Krk-scheme PDFs for the former.

Due to the low jet-identification p_T -cut used, and the falling $d\sigma/dp_T^j$ distribution, the $d\sigma/dy_j$ distribution is dominated by the normalisation differences implied by the discussion of the low- p_T^j region above. The KrkNLO distribution again lies outside the MC@NLO matching uncertainty envelope, for the same reason, due to the relative suppression in the low- $p_T^{j_1}$ which dominates the distribution. The shapes of the rapidity distributions are broadly comparable, with the exception of the WW process.

Turning to the inclusive distributions shown in fig. 4, the differential cross-section with respect to the invariant mass of the colour-singlet system is dominated by the low- p_T region (as shown in fig. 6) in which the Sudakov factor and Krk PDFs suppress the KrkNLO prediction relative to the others (see also the discussion of $d\sigma/dp_T^{j_1}$ above).¹⁵ At intermediate- p_T , the lower peak of the invariant-mass distribution for the $Z\gamma$ process allows the difference in shower-scale within the MC@NLO alternatives to generate greater radiation below the $d\sigma/dM_{\ell\ell\gamma}$ -peak. At high- p_T the invariant-mass distributions generally converge between the NLO-accurate predictions.

Overall, due to the shape of the $d\sigma/dM$ distributions, especially for the ZZ and WW processes, there is relatively limited opportunity for the starting-scale difference between the invariant mass of the colour-singlet system (in the ‘DGLAP’/‘default’ case) and the kinematic upper-limit (in the ‘power’ case) to contribute to matching uncertainty at this level. The uncertainty envelope obtained by shower-scale variation within the MC@NLO method is therefore negligible, for the three choices considered here, and so underestimates the true matching-uncertainty at one-emission level.

Considering the azimuthal angle between particles within the colour-singlet system, shown in fig. 4, the KrkNLO method best reproduces the NLO fixed-order distributions away from the back-to-back limit in which perturbation theory breaks down ($\Delta\phi \rightarrow \pi$), while the effect of the low- p_T suppression of the KrkNLO method is again visible close to the back-to-back region. The high- p_T effect of the power-shower discussed above, due to recoil against a hard emission, can again here be

¹⁴This difference is attributable to ‘S’-events in which the transverse momentum of the first-emission exceeds the invariant mass of the colour-singlet system, as can be seen from fig. 6.

¹⁵See also the corresponding full-shower plots of fig. 7 and the accompanying discussion for the effect of the subsequent radiation.

seen to affect the $\Delta\phi$ distribution, generating a large matching-uncertainty within the MC@NLO method at low- $\Delta\phi$.

The rapidity-separation, by contrast, shows good agreement within the MC@NLO predictions and between the MC@NLO predictions and fixed-order NLO. The low- p_T Sudakov suppression discussed above again leads to a normalisation difference across the distribution for the KrkNLO method, which increases slightly at large rapidities.

4.2 Full shower

Differential cross-sections for the invariant mass of the colour-singlet system, and the azimuthal angle and rapidity separations between the two particles in the imputed $2 \rightarrow 2$ final-state, are shown in fig. 10; differential cross-sections for the transverse momentum and rapidity of the leading jet are shown in fig. 11. As in the one-emission case, to elucidate the role of QCD radiation across the inclusive phase-space, differential cross-sections $d\sigma/dM$ in slices of $p_T^{j_1}$ are presented in fig. 7. Additionally, following the approach of [27], $d\sigma/dM$ and $d\sigma/dp_T^{j_1}$ further divided into six equal slices of the azimuthal separation between the particles within the imputed two-body colour-singlet final-state are shown in fig. 8 and fig. 9 respectively.

The Born-like kinematics corresponds to $p_T^{j_1} \rightarrow 0$ and $\Delta\phi \rightarrow \pi$, and so these limits parametrise the break-down of perturbation theory for fixed-order calculations. In this limit, the parton shower provides all-orders resummation. Far from this limit, the colour-singlet system recoils against hard QCD radiation. Close to it, the kinematic configuration is effectively Born-like, with only relatively soft QCD radiation.

Overall, the distributions in fig. 10 show good agreement between the methods, with the deviation between KrkNLO and the conventional MC@NLO variants ('default' and 'DGLAP') typically smaller than 20% and often significantly smaller. This is generally smaller than the uncertainty within the MC@NLO method due to the choice of shower starting-scale, as illustrated by the large deviations for the power-shower variant of MC@NLO. The deviations appear to shrink with effective mass-scale, with the ZZ process showing very little matching uncertainty in any distribution.

Figures 7 and 8 show that in the hard-emission region, the KrkNLO method generally gives results lying within the MC@NLO uncertainty envelope, and generally lying close to the 'default' and DGLAP MC@NLO variants. A similar picture can be seen from the small-azimuthal-separation regime in fig. 9.

In the resummation region, the differences are much smaller than at one-emission, with relatively close agreement between the predictions shown in figs. 7 and 8. However, larger differences are visible in the $d^2\sigma/d\phi dp_T^{j_1}$ distributions, which isolate the resummation region simultaneously in angle and in transverse momentum. Here the KrkNLO method consistently lies outwith the envelope of the other predictions, but with distinctive shape similarities between the 'default' MC@NLO variant and KrkNLO for both W and WW , also observed in the diphoton case in [27]. The low- $p_T^{j_1}$, large- $\Delta\phi$ region dominates each process; for many experimental analyses with typical jet cuts, this region would correspond to (and dominate) events with no identified jets. The scale below which the difference in Sudakov suppression in the low- $p_T^{j_1}$ region emerges is approximately $p_T^{j_1} < 20$ GeV for WW and ZZ , $p_T^{j_1} < 50$ GeV for W , and $p_T^{j_1} < 80$ GeV for $Z\gamma$. That the matching uncertainty is concentrated in the low- p_T , back-to-back region is perhaps unsurprising, since this is the region in which the perturbative constraints on higher-order terms are confronted with large logarithms arising from the parton shower. However, this is also the region of phase-space in which the uncertainty envelope arising from shower-scale variation within the MC@NLO method collapses, due to the low emission-scale being permitted irrespective of the functional-form chosen for the starting-scale.

Since the overall matching uncertainty is dominated by the soft-emission phase-space region in which shower-scale variation is inconsequential, variation within the MC@NLO method is insufficient and the comparison of alternative methods is necessary.

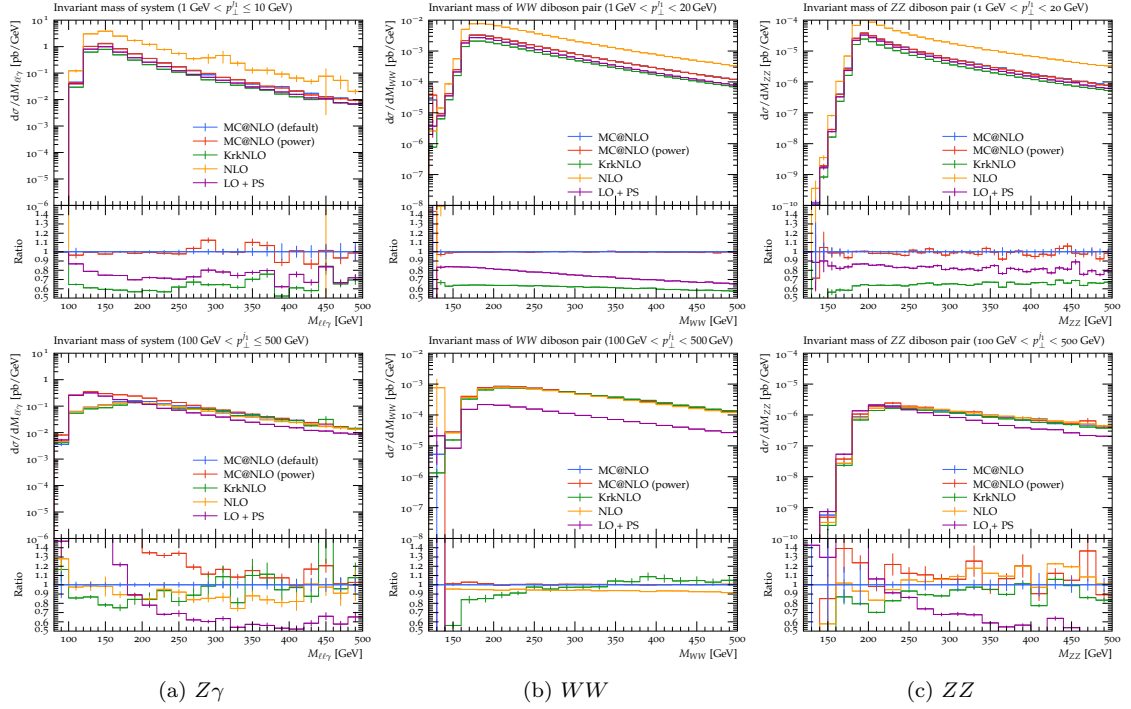


Figure 6: ‘Parton-level’ (first-emission) comparison of the invariant mass of the colour-singlet system in ‘soft’ and ‘hard’ slices of the transverse momentum of the leading jet. The full-shower counterpart is shown in fig. 7. The complete array of double-differential slices is shown in fig. 18.

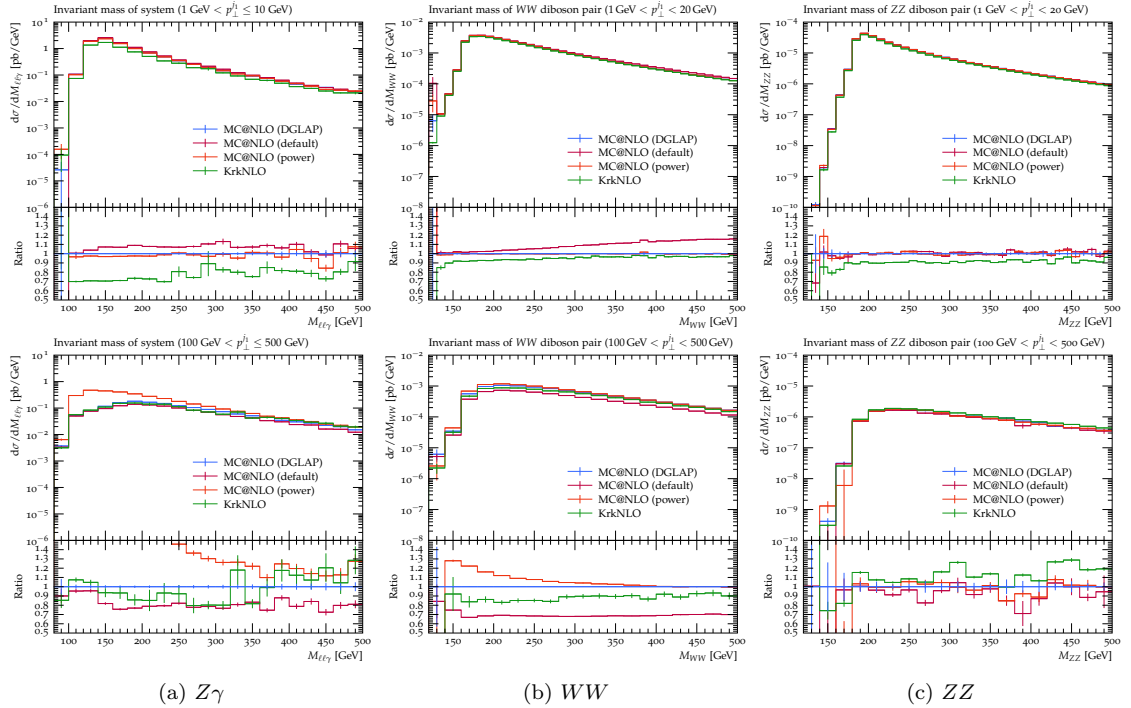


Figure 7: Full-shower comparison of the invariant mass of the colour-singlet system for ‘soft’ and ‘hard’ slices of the transverse momentum of the leading jet. The one-emission counterpart is shown in fig. 6. The complete array of double-differential slices is shown in fig. 19.

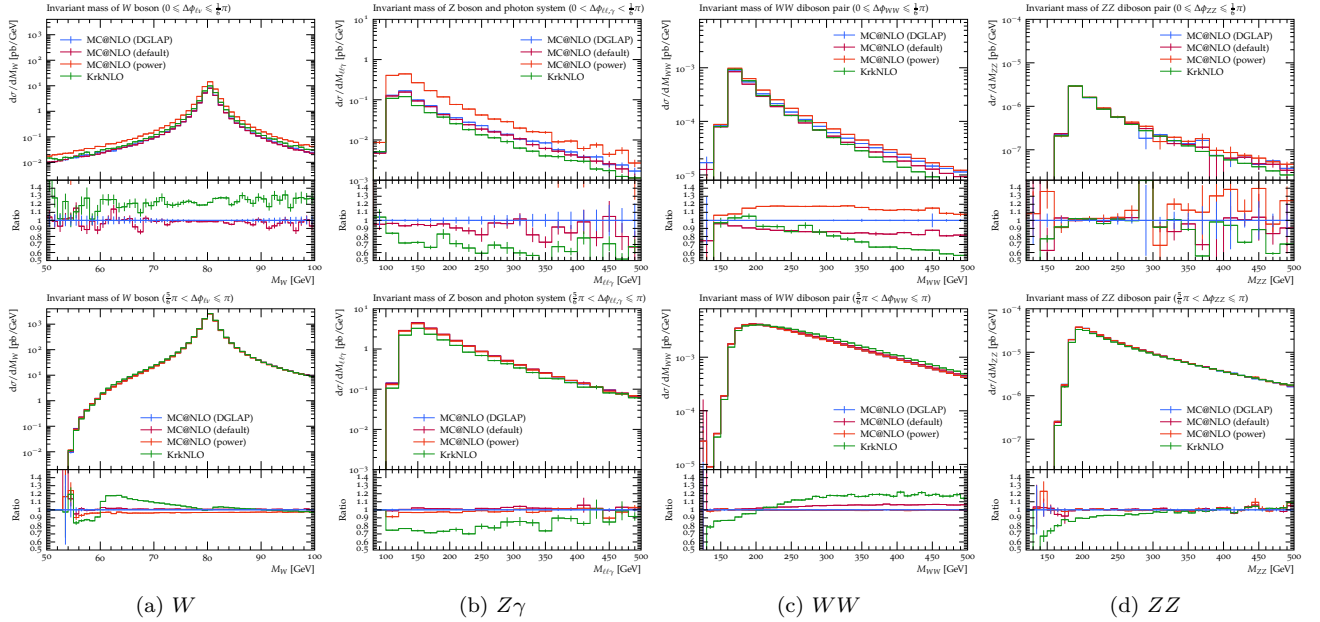


Figure 8: Full-shower comparison of the invariant mass of the colour-singlet system in slices of the azimuthal angle between the (reconstructed) two-particle constituents of the colour-singlet system, for ‘hard’ and ‘soft’ (respectively) radiation. The complete array of double-differential slices is shown in fig. 20.

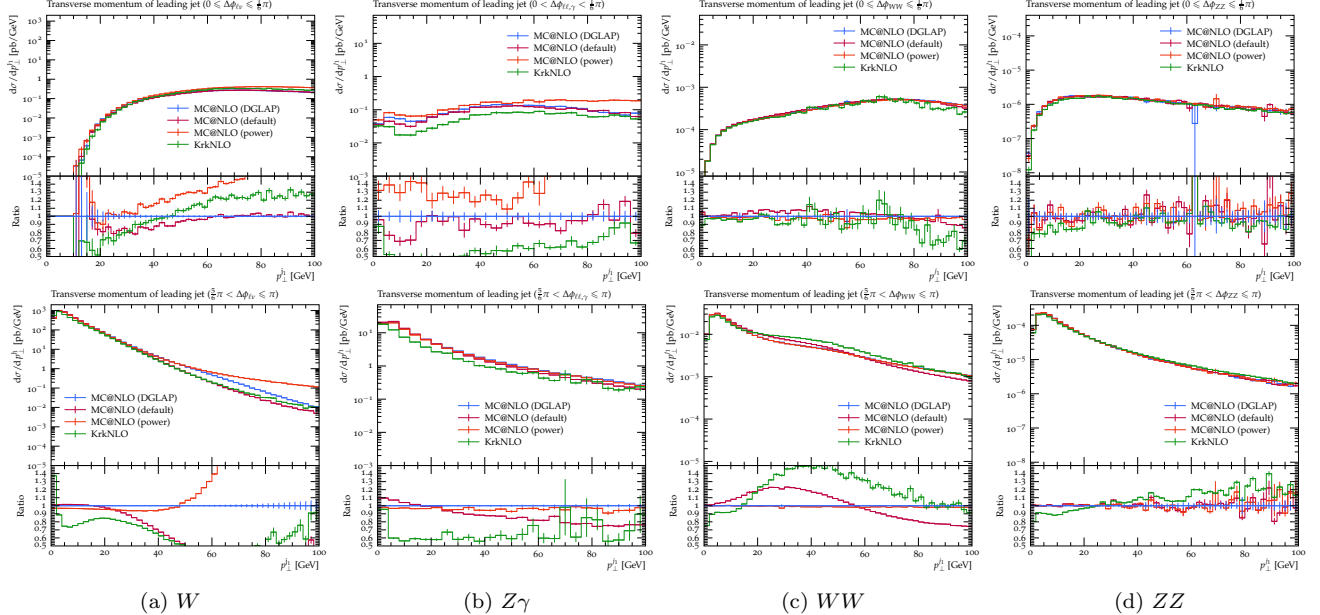


Figure 9: Full-shower comparison of the transverse momentum of the leading jet in slices of the azimuthal angle between the (reconstructed) two-particle constituents of the colour-singlet system, for ‘hard’ and ‘soft’ (respectively) radiation. The complete array of double-differential slices is shown in fig. 21.

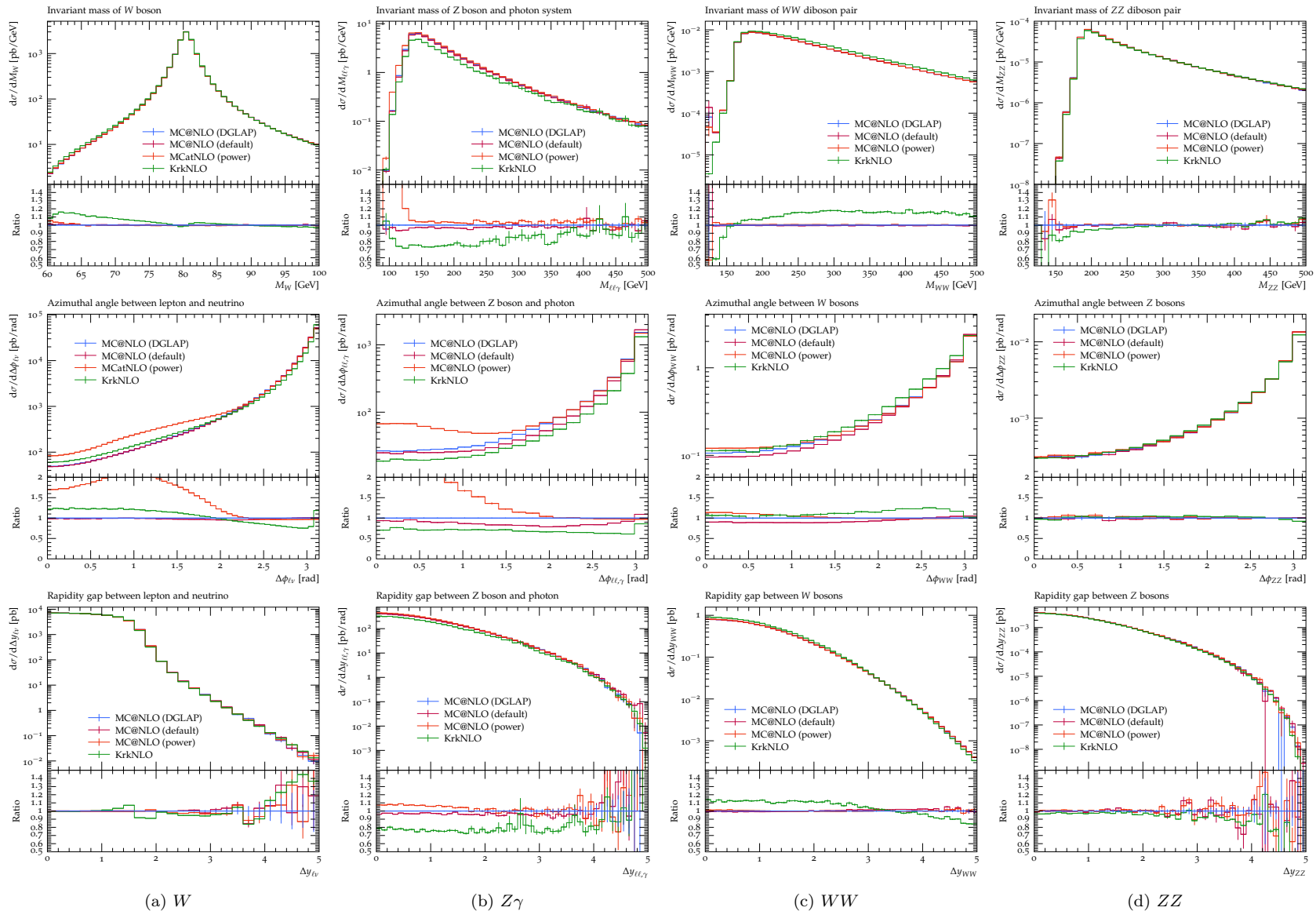


Figure 10: Full-shower comparison of the inclusive distributions. The one-emission counterpart is shown in fig. 4.

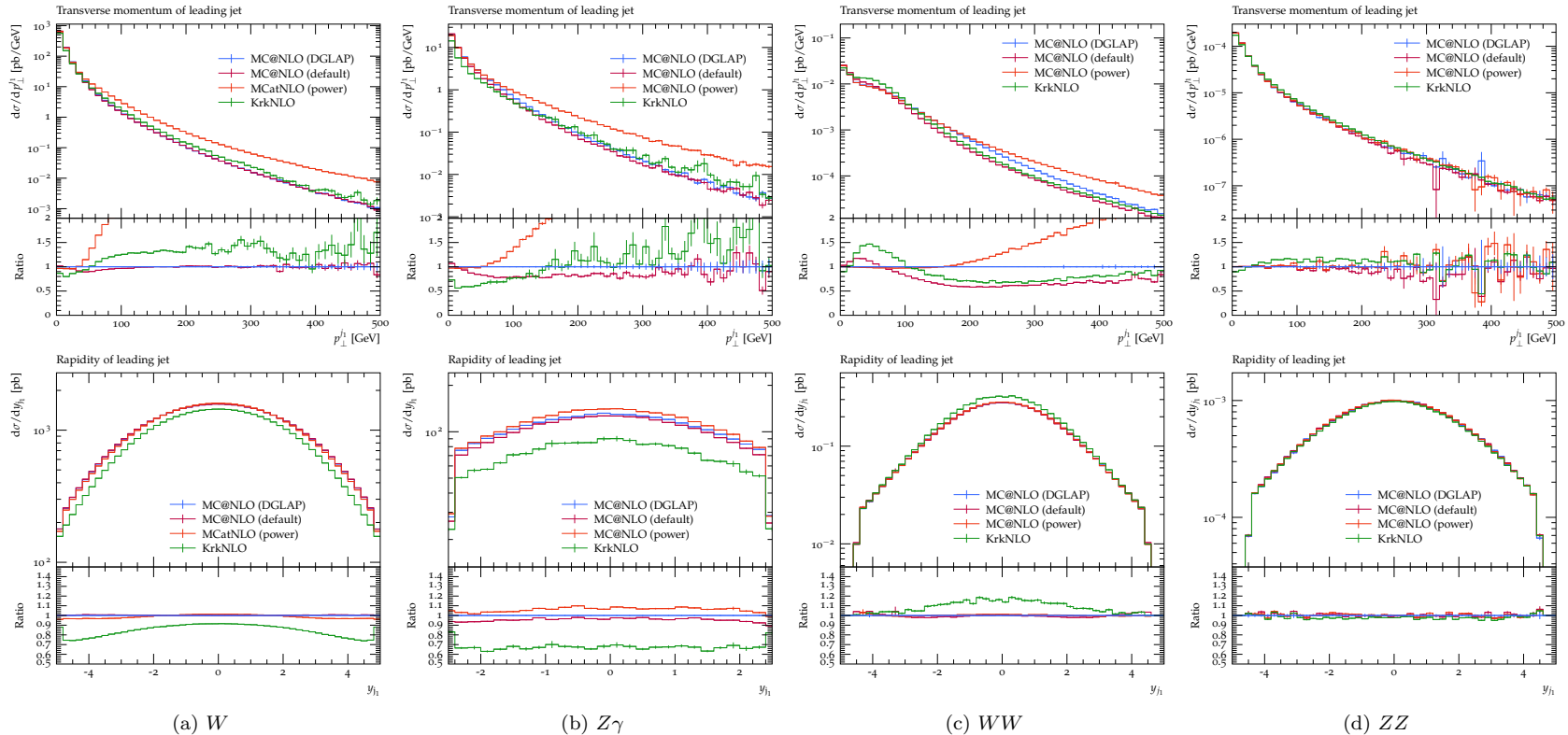


Figure 11: Full-shower comparison of the leading-jet distributions. The one-emission counterpart is shown in fig. 5.

5 LHC phenomenology

In this section we use the same runs as in section 4, and apply analyses previously used for LHC data. These are therefore histograms of the same events from the same simulations, but with different cuts and observable binnings. In particular, rather than cuts and observables chosen for consistent inter-process comparison, they reflect choices made for experimental purposes for each process independently.

For each process, we summarise the current theoretical status and the expected size of the missing, but known, higher-order-corrections. We then contextualise The differences between the matching methods, and resulting matching uncertainty, can therefore be contextualised with respect to the missing higher-order corrections, the observed level of agreement with data, and the experimental uncertainty.

5.1 Charged-current Drell–Yan

The charged-current Drell–Yan process has been calculated to $N^3\text{LO}$ accuracy in QCD [49–52], and at NNLO+PS in the UN^2LOPS [10], NNLOPS post-hoc reweighting [53], GENEVA [54] and MiNNLOPS [11] formalisms. The magnitude of QCD corrections beyond NLO is relatively small. The $W + j$ process has been calculated to NNLO accuracy in QCD [55–58]; the NLO local K -factor for $d\sigma/dp_T^{j_1}$ is approximately 50%, while the NNLO corrections are much smaller in magnitude.

We use the generation parameters of table 1 and the experimental cuts of [59]

$$p_T^\ell > 20 \text{ GeV}, \quad |\eta^\ell| < 2.5, \quad (5.1\text{a})$$

$$E_T^{\text{miss}} > 25 \text{ GeV}, \quad m_T^W > 40 \text{ GeV}, \quad (5.1\text{b})$$

and [60]

$$p_T^\ell > 25 \text{ GeV}, \quad |\eta^\ell| < 2.5, \quad (5.2\text{a})$$

$$E_T^{\text{miss}} > 25 \text{ GeV}, \quad m_T^W > 40 \text{ GeV}, \quad (5.2\text{b})$$

$$p_T^j > 30 \text{ GeV}, \quad |y^{\text{jet}}| < 4.4, \quad \Delta R_{\ell j} > 0.5, \quad (5.2\text{c})$$

as implemented in the `ATLAS_2011_I928289_W` and `ATLAS_2014_I1319490` analyses within `Rivet` [36] respectively. The resulting plots are shown in fig. 12.

We observe very little matching uncertainty in the inclusive distributions of fig. 12a, all of which describe the data to a comparable level (approximately 5%). The KrkNLO method consistently describes the charge-asymmetry within experimental uncertainties across the pseudorapidity distribution; all methods agree within 10%. The jet distributions of fig. 12b show greater matching uncertainty, as expected from their formal LO-accuracy and the discussion in section 4.

The KrkNLO predictions can again be seen to lie within the matching uncertainty envelope of the `Mc@NLO` method, and generally between the ‘default’ and ‘DGLAP’ shower-scale variants. Although the ‘power’-shower variant appears to achieve the correct normalisation in the jet-rapidity distribution, this is an artefact of the tail of the $p_T^{j_1}$ -distribution, as in section 4.

5.2 $Z\gamma$ production

The $Z\gamma$ process has been calculated to NNLO accuracy in QCD [61–63], and at NNLO+PS in the `MiNNLOPS` [64] formalism. The NNLO corrections are of the order of 20%. The NLO EW corrections [65] become significant at large values of the invariant mass $M_{\ell\ell\gamma}$.

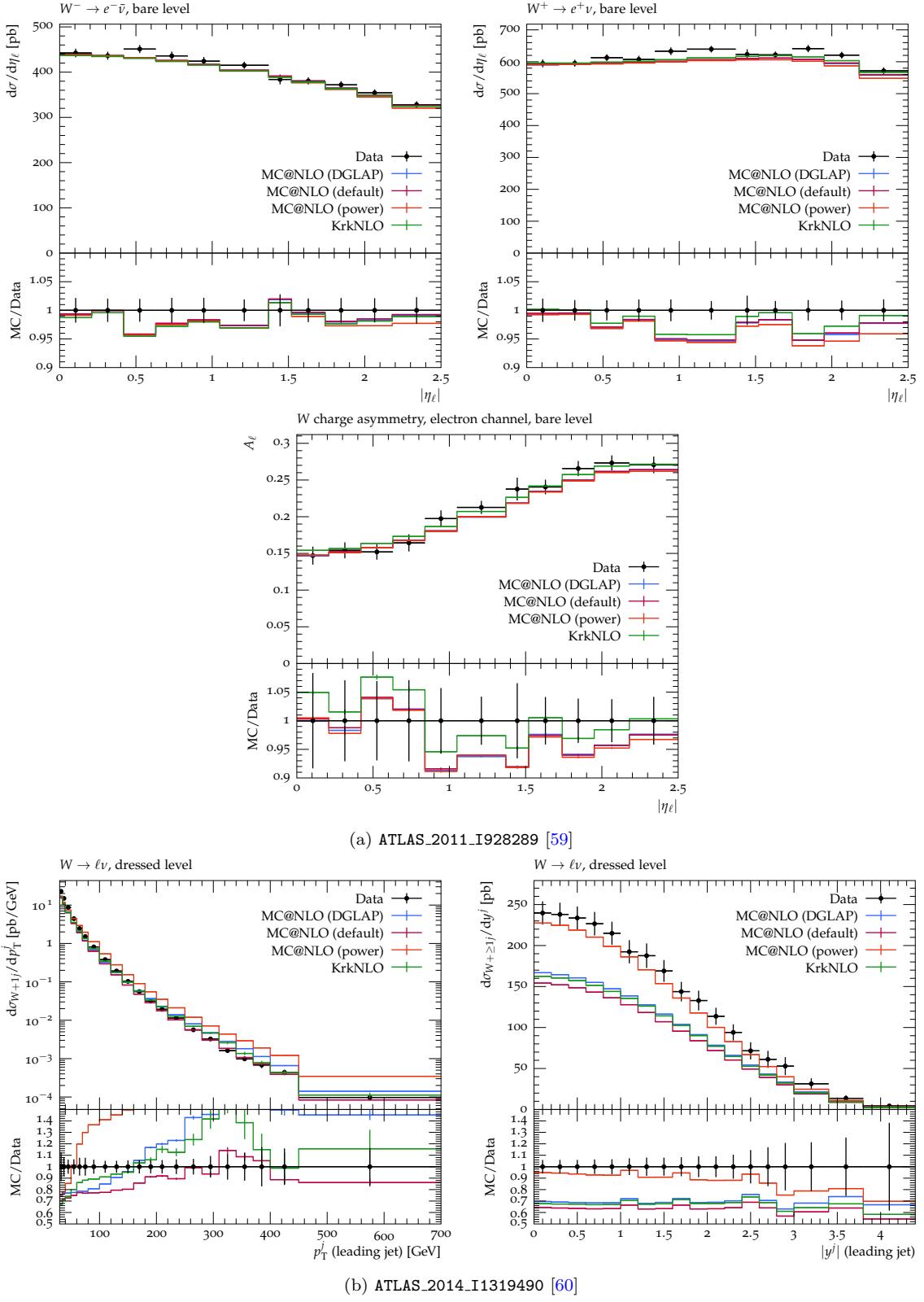


Figure 12: W : Comparison of matched NLO-plus-parton-shower differential cross-sections as generated by KrkNLO and MC@NLO, to 7 TeV ATLAS data from [59, 60]. Note that the experimental results of fig. 12a are averaged over lepton-flavour, and only the unfolding is flavour-specific. The jet distributions in fig. 12b are formally of LO accuracy.

We again use the generation parameters of table 1 and the experimental cuts of [66]

$$p_T^{\ell_1} > 30 \text{ GeV}, \quad p_T^{\ell_2} > 25 \text{ GeV}, \quad |\eta^\ell| < 2.47, \quad (5.3a)$$

$$p_T^\gamma > 30 \text{ GeV}, \quad |\eta^\gamma| < 2.37, \quad (5.3b)$$

$$M_{\ell\ell} > 40 \text{ GeV}, \quad \Delta R_{\ell\gamma} > 0.4, \quad M_{\ell\ell} + M_{\ell\ell\gamma} > 182 \text{ GeV}, \quad (5.3c)$$

$$E_T^{\text{iso}}(r) < 0.07 p_T^\gamma \quad \text{within cone } r \leq R = 0.2, \quad (5.3d)$$

as implemented in the Rivet analysis ATLAS_2019_I1764342. The resulting plots are shown in fig. 13.

As expected from the general observations of section 4, in the $Z\gamma$ case we see substantial matching uncertainty. Between the methods, neither MC@NLO nor KrkNLO is consistent with the data across phase-space. The data lies within the overall matching uncertainty envelope save for the intermediate- $p_{T,\ell\ell\gamma}$ region where additional real-radiation is expected to be significant. As in section 4, but unlike the other processes studied here, the KrkNLO prediction generally lies outwith the MC@NLO uncertainty envelope, likely again due to the Sudakov factor accompanying the (abundant) soft emissions. In regions of phase-space characterised by hard recoil, this is absent.

Again, although the power-shower variant of MC@NLO agrees with data in certain distributions, the shape difference observed in the $d\sigma/d\Delta\phi_{\ell\ell,\gamma}$ distribution in section 4 leads to a substantial overestimate relative to the data at low- $\Delta\phi_{\ell\ell,\gamma}$. The apparent agreement in the normalisation of the MC@NLO predictions is in tension with the known magnitude of the missing NNLO corrections.

5.3 WW production

The WW process has been calculated to NNLO accuracy in QCD [67, 68] including with polarised W -bosons [69], and at NNLO+PS in the NNLOPS post-hoc reweighting [70], MiNNLOPS [71], and GENEVA [72] formalisms. The NNLO correction changes the total cross-section by approximately 15% relative to NLO [68], around half of which is attributable to the gg -channel. The NLO EW corrections [73] become significant at large values of the invariant mass M_{WW} .

We use the generation parameters of table 1 and the experimental cuts of [74], which select for two opposite-charge, different-flavour leptons within fiducial cuts

$$p_T^\ell > 27 \text{ GeV}, \quad |\eta^\ell| < 2.5, \quad (5.4a)$$

$$p_T^{\text{miss}} > 20 \text{ GeV}, \quad (5.4b)$$

$$M_{\ell\ell'} > 55 \text{ GeV}, \quad p_T^{\ell\ell'} > 30 \text{ GeV}, \quad (5.4c)$$

as implemented in the Rivet analysis ATLAS_2019_I1734263. The resulting plots are shown in fig. 14.

For the WW process, we observe a reduced matching uncertainty, as in section 4. The KrkNLO distributions once again lie within the MC@NLO envelope, and generally closest to the ‘default’-shower MC@NLO variant. The data is consistent with the matched NLO predictions within the matching-uncertainty envelope, save for the $d\sigma/dp_{T,\ell_1}$ distribution at intermediate- p_{T,ℓ_1} .

5.4 ZZ production

The ZZ process has been calculated to NNLO accuracy in QCD [75–78] including recently with polarised Z -bosons [79], and at NNLO+PS in the GENEVA [80] and MiNNLOPS [81] formalisms. The NNLO correction changes the total cross-section by approximately 20% relative to NLO [78], around half of which is attributable to the gg -channel which opens up at NNLO. In turn, the gluon-initiated channel itself receives significant NLO (respectively, N^3LO) corrections [82]. The NLO EW corrections [73] become significant at large values of the invariant mass M_{ZZ} .

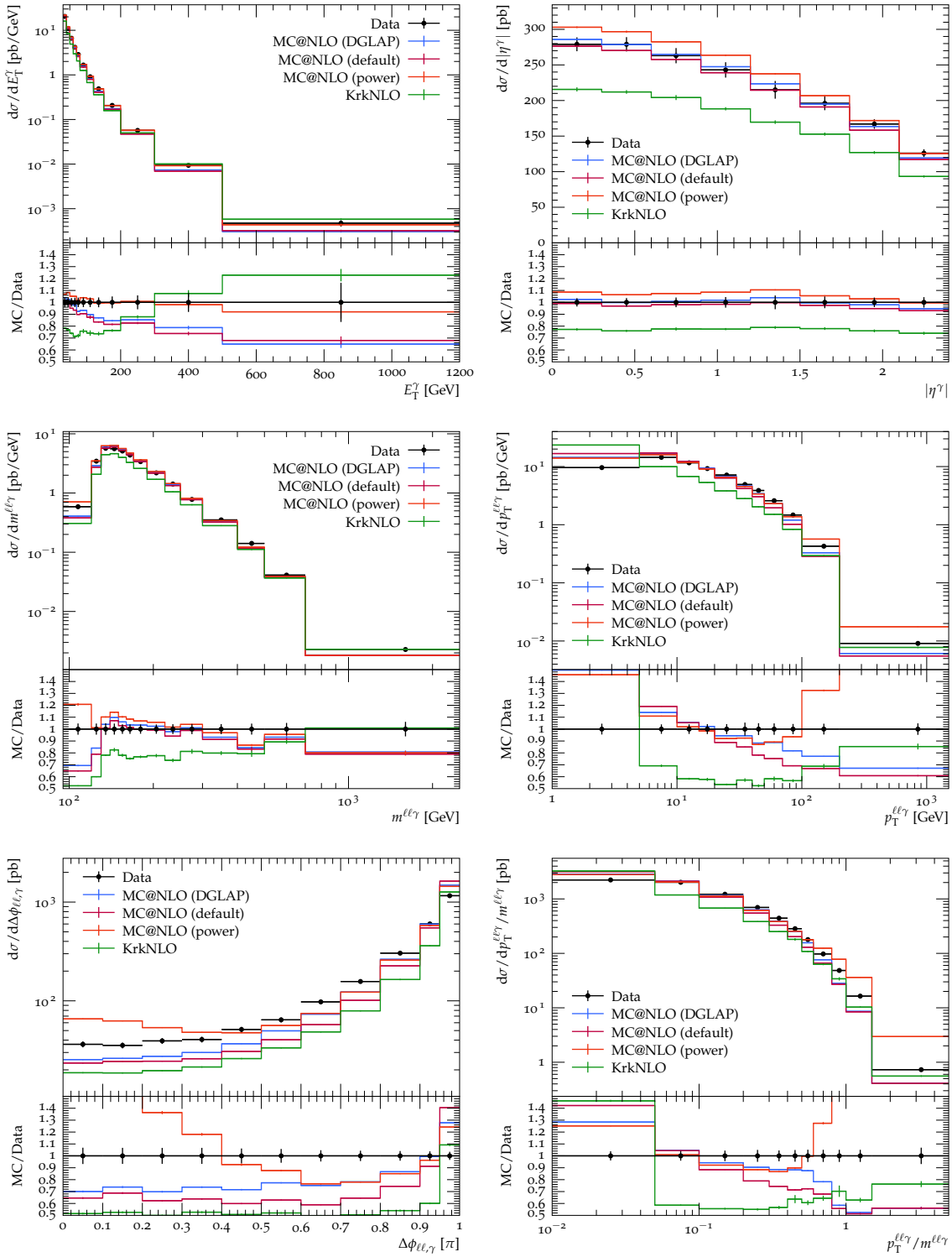


Figure 13: $Z\gamma$: Comparison of matched NLO-plus-parton-shower differential cross-sections as generated by KrkNLO and MC@NLO, to 13 TeV ATLAS data from [66]. Note that the first three distributions are formally calculated to NLO accuracy, while the last three are LO.

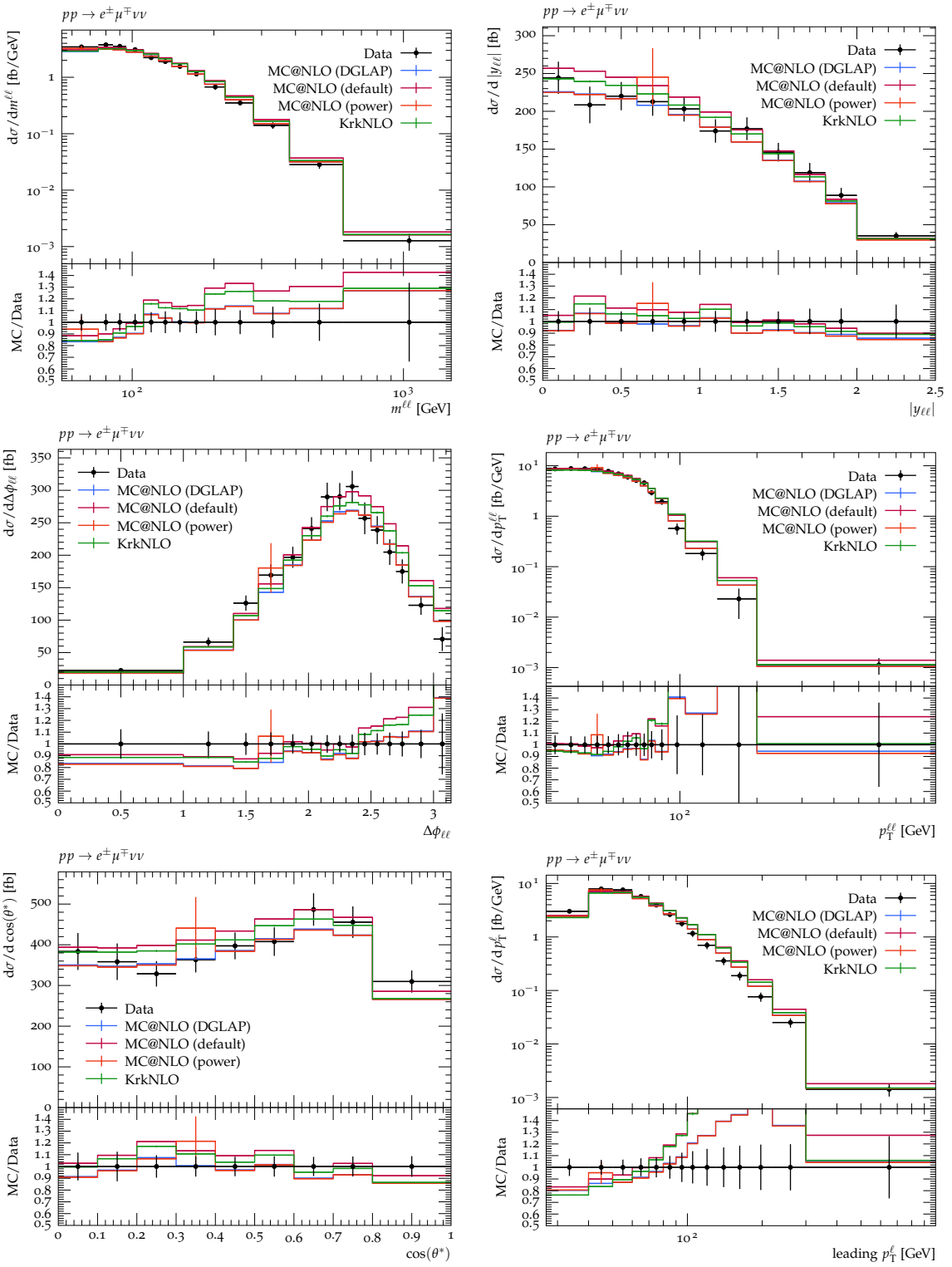


Figure 14: WW : Comparison of matched NLO-plus-parton-shower differential cross-sections as generated by KrkNLO and Mc@NLO, to 13 TeV ATLAS data from [74].

We use the generation parameters of table 1 and the experimental cuts of [83], which selects for two pairs of same-flavour, opposite-charge leptons within fiducial cuts¹⁶

$$(p_T^{\ell_1}, p_T^{\ell_2}, p_T^{\ell_3}, p_T^{\ell_4}) > (20, 15, 10, 5) \text{ GeV}, \quad |\eta^\ell| < 2.7, \quad (5.5a)$$

$$M_{Z_1 Z_2} \in (66, 116) \text{ GeV}, \quad M_{\ell^+ \ell^-} > 5 \text{ GeV}, \quad (5.5b)$$

implemented in the Rivet analysis ATLAS_2017_I1625109. The resulting plots are shown in fig. 15.

Again, as discussed in section 4 we observe very limited matching-uncertainty between our matched-NLO predictions, none of which describes the data, as might be expected from the NNLO K -factor of [75–78]. The results of [76] imply that the shape of distributions changes relatively little between NLO and NNLO, only the normalisation.

6 Conclusions

In this paper we have presented the extension of the KrkNLO implementation within `Herwig` to support the full class of processes calculable with the method. We applied this to four characteristic LHC processes, and investigated the matching uncertainty of the resulting predictions, as compared with three variants of the standard `Mc@NLO` method. By performing double-differential comparisons consistently across processes, we can assess the numerical effect of the formal differences between the alternative matching algorithms.

We find generally consistent predictions between the methods, with the KrkNLO predictions mostly lying within the `Mc@NLO` uncertainty envelope, and closest to the ‘default’ shower-scale choice within `Herwig`. For processes and observables very sensitive to additional radiation, the ‘power’-shower variant of the `Mc@NLO` method inflates the `Mc@NLO` matching uncertainty, leading to a wide matching-uncertainty band for inclusive observables. In other regions of phase-space the KrkNLO method provides a complementary prediction, indicating that shower-scale variation within the `Mc@NLO` method alone underestimates the overall matching uncertainty. The generally good level of agreement between the ‘default’ `Mc@NLO` scale choice and the predictions of the KrkNLO method provides empirical justification for its use as the default.

For many of the processes considered, NLO predictions are insufficient to describe the full range of LHC data, due to missing contributions including the neglected gg -channel. Additionally, within the KrkNLO method, there is an additional suppression arising from the parton-shower Sudakov factor. As we pursue the further extension of the KrkNLO method to higher levels of formal accuracy, the numerical significance of this Sudakov suppression should be reduced. We expect that the insights gleaned from this detailed process-by-process comparison will prove useful and inform this work.

Acknowledgments

The authors wish to thank Wiesław Płaczek and the late Stanisław Jadach for their work on, and for many fruitful discussions about, the KrkNLO method. We are grateful to Wiesław Płaczek for comments on the manuscript.

This work was supported by grant 2019/34/E/ST2/00457 of the National Science Centre, Poland. AS is also supported by the Priority Research Area Digiworld under the program ‘Excellence Initiative – Research University’ at the Jagiellonian University in Krakow. AS thanks the CERN Theoretical Physics department for hospitality while part of this research was being carried out. We gratefully acknowledge Polish high-performance computing infrastructure PLGrid (HPC Centre: ACK Cyfronet AGH) for providing computer facilities and support within computational grants PLG/2024/017934 and PLG/2025/018065.

¹⁶Full details of the fiducial phase-space and boson reconstruction procedure from the four-lepton final-state are given in [83].

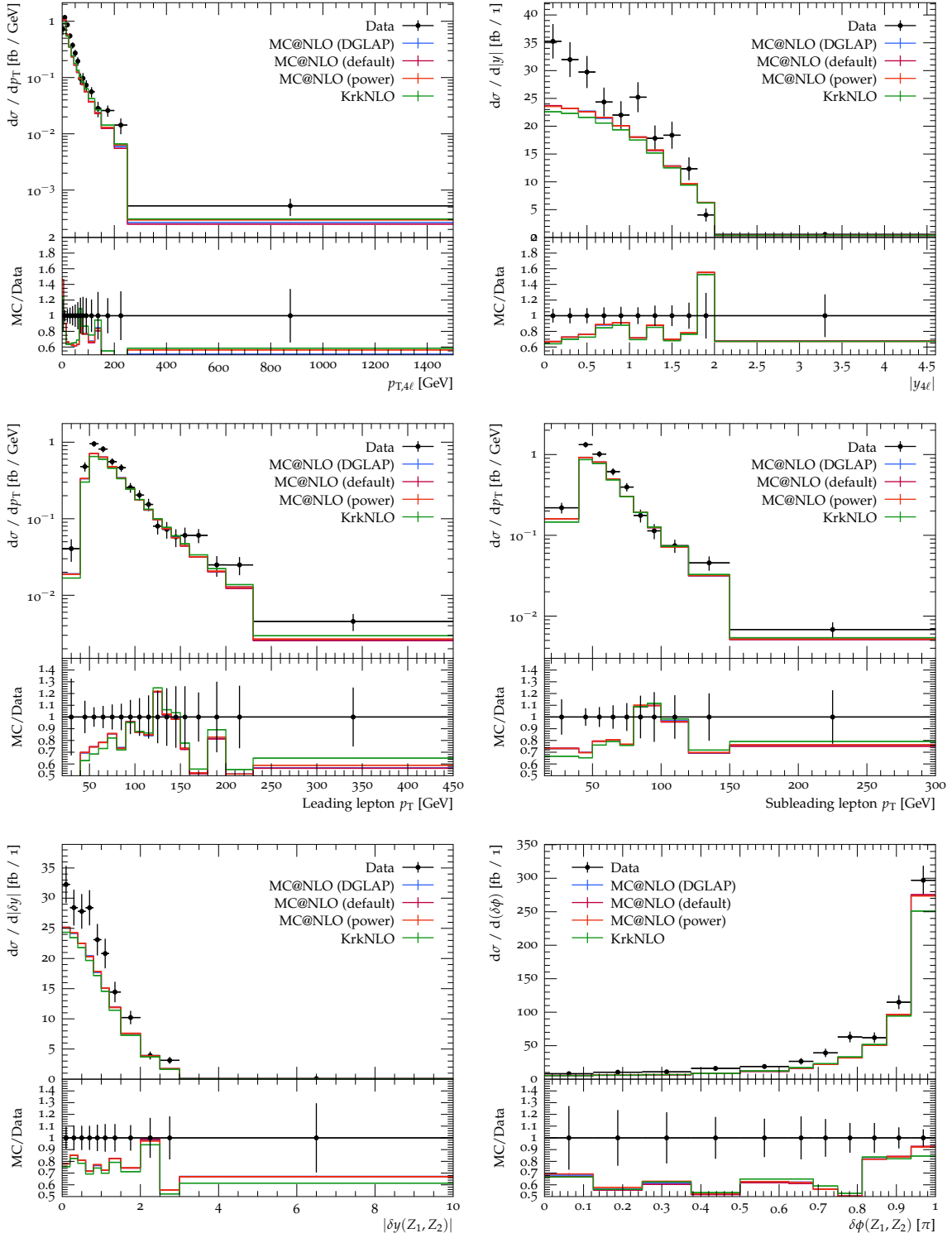


Figure 15: ZZ : Comparison of matched NLO-plus-parton-shower differential cross-sections as generated by KrkNLO and MC@NLO, to 13 TeV ATLAS data from [83].

A Positivity of KrkNLO event-weights

The KrkNLO method is formulated to generate only positive-weights by construction, subject to the Krk-scheme PDFs being positive,¹⁷ and the positivity of the virtual reweight. Because it does not use subtraction, there is no risk of negativity caused by over-subtraction, which is a common source of negative event-weights in MC@NLO. As outlined for example in [7], in regions of phase-space in which perturbation theory breaks down, large and negative virtual matrix-elements can, despite their formal suppression within the α_s -expansion, render the Φ_m -contribution locally-negative.

Within the KrkNLO method, as summarised in section 2, the virtual reweight includes an additional virtual-like contribution Δ_0^{FS} compensating the $\delta(1-x)$ terms introduced within the PDF transformation from the $\overline{\text{MS}}$ to the Krk-scheme,

$$1 + \frac{\alpha_s(\mu_R)}{2\pi} \left(\frac{V(\Phi_m; \mu_R)}{B(\Phi_m)} + \frac{I(\Phi_m; \mu_R)}{B(\Phi_m)} + \Delta_0^{\text{FS}} \right). \quad (\text{A.1})$$

For the Krk-scheme, these terms are fixed by the choice to impose the $\overline{\text{MS}}$ momentum-conservation sum-rule [84]

$$\sum_a \int_0^1 \xi f_a^{\text{FS}}(\xi, \mu) d\xi = 1 \quad (\text{A.2})$$

on the Krk-scheme PDFs,¹⁸ which leads to [27]

$$\Delta_0^{\text{Krk}} = C_F \left(2\pi^2 - \frac{3}{2} \right) \approx 24.3189. \quad (\text{A.3})$$

Since this is large and positive, it has the effect of further mitigating negativity even in regions of phase-space where a negative virtual matrix-element alone would ‘overpower’ the positivity of the Born matrix-element in isolation. As an indicative value, $\Delta_0^{\text{Krk}} \alpha_s(M_Z)/2\pi \approx 0.46$.

In fig. 16 we show the empirical weight-distributions obtained from the generator set-up used for sections 4.2 and 5, prior to the analysis cuts. In fig. 17 we show the differential cross-section with respect to the event weight. As can be seen from the weight distributions, within the KrkNLO method the problem of negative weights is almost entirely eliminated, with a small number visible in the bin adjoining 0 in fig. 16 (though not fig. 17, due to their vanishing contribution to the cross-section). This is in contrast with the MC@NLO predictions, which show the characteristic weight-distributions of subtractive calculations.

We illustrate the origin of these negative weights by also showing equivalent KrkNLO runs made using explicitly non-negative PDF sets.¹⁹ These results confirm that weight-negativity observed in the KrkNLO method for these processes is almost entirely attributable to the negativity of the transformed Krk-scheme CT18NLO PDF set in certain corners of (x, Q) -space, as explored in [35]. For practical purposes both choices can be seen to have negligible event-weight-negativity, for these processes, and therefore to provide a solution to the negative-weight problem in event generation.

B Unabridged double-differential distributions

For completeness, we here reproduce the double-differential distributions presented in the main text in their full context, with no omitted phase-space ‘slices’. For each distribution, the processes

¹⁷See [35] for a study of the positivity properties of alternative factorisation schemes, including the Krk scheme.

¹⁸The significance of this choice, for a number of alternative factorisation schemes, is explored in [35].

¹⁹In practice, we achieve this using the `ForcePositive` switch within the LHAPDF library for CT18NLO in the Krk scheme, and the positive-definite NNPDF40MC PDF set for the shower.

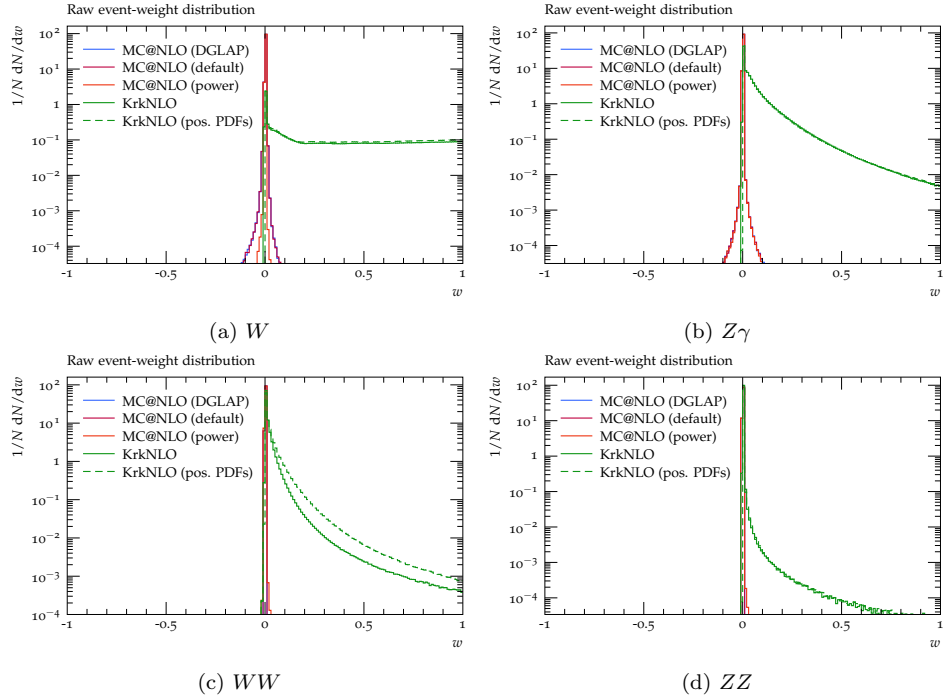


Figure 16: Event-weight distributions of the KrkNLO and MC@NLO methods, for the generator set-up used for the predictions in sections 4.2 and 5. Note that only the generation cuts of table 1 have been applied, and no analysis cuts.

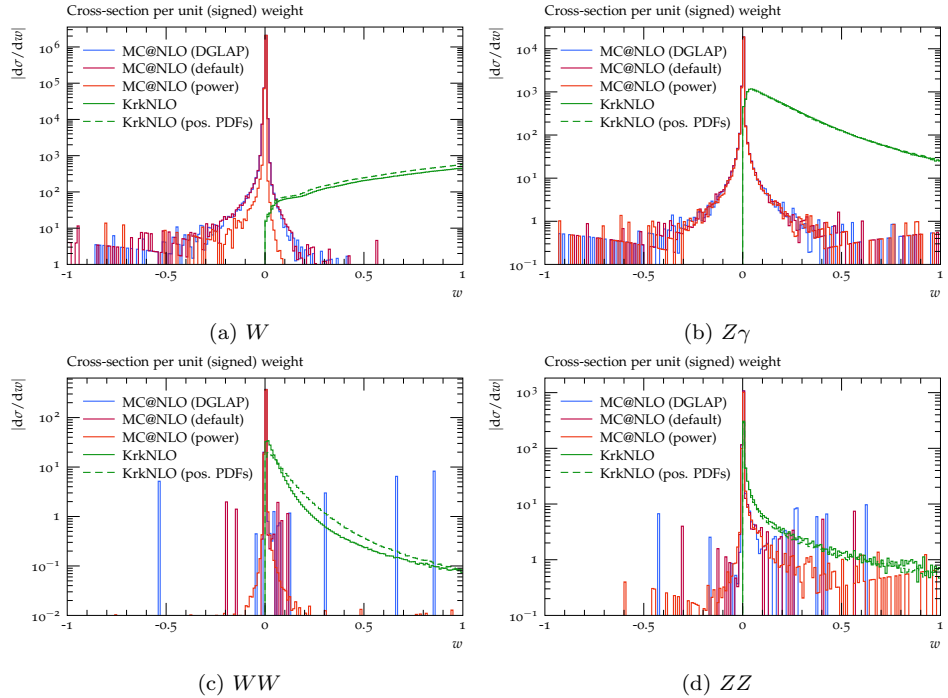


Figure 17: Magnitude of the differential cross-section with respect to event weight for the KrkNLO and MC@NLO methods, for the generator set-up used in sections 4.2 and 5. Note that only the generation cuts of table 1 have been applied, and no analysis cuts.

are presented left-to-right in a consistent order, while adjacent slices in the second observable are presented top-to-bottom. In figs. 20 and 21, for which the second observable is $\Delta\phi$, the slices partition the inclusive phase-space, so that every event passing the fiducial cuts contributes to exactly one $\Delta\phi$ interval. In figs. 18 and 19, for which the second observable is $p_T^{j_1}$, the slices partition the radiative phase-space, omitting only events for which the parton shower evolution generates no radiation.

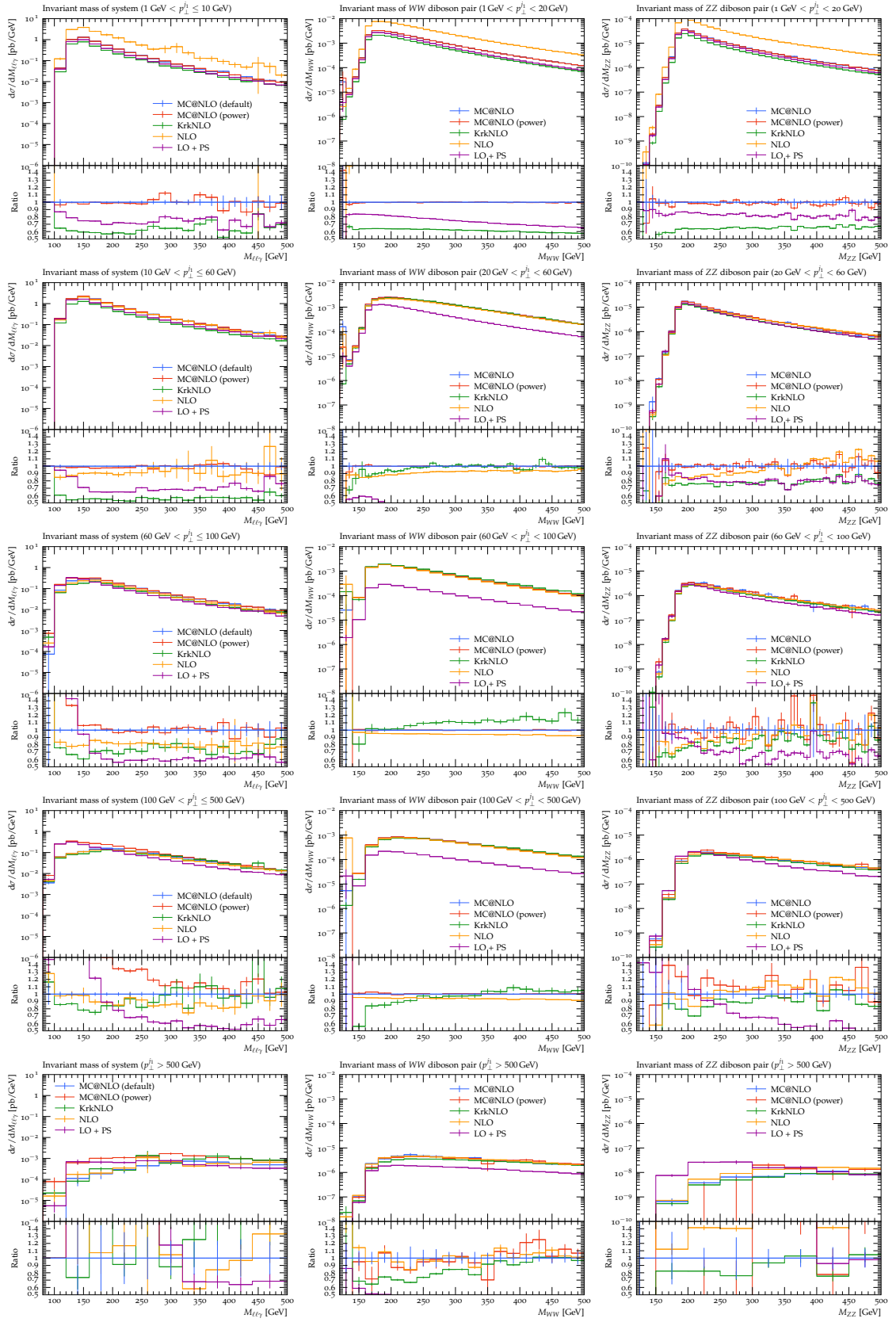
(a) $Z\gamma$ (b) WW (c) ZZ

Figure 18: ‘Parton-level’ (first-emission) comparison of the invariant mass of the colour-singlet system in slices of the transverse momentum of the leading jet; the complete partition of which a subset is shown in fig. 6.

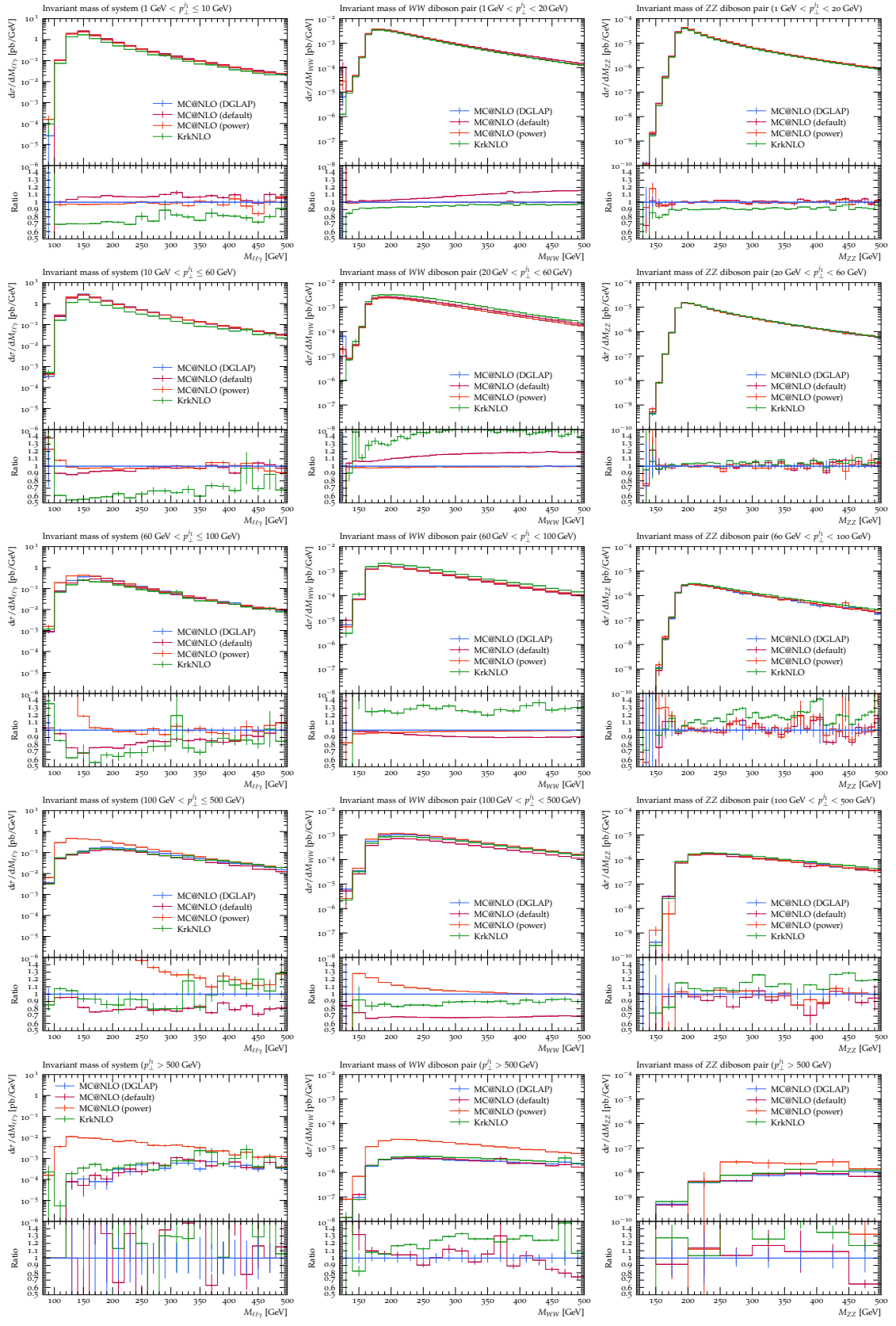


Figure 19: Full-shower comparison of the invariant mass of the colour-singlet system in slices of the transverse momentum of the leading jet; the complete partition of which a subset is shown in fig. 7.

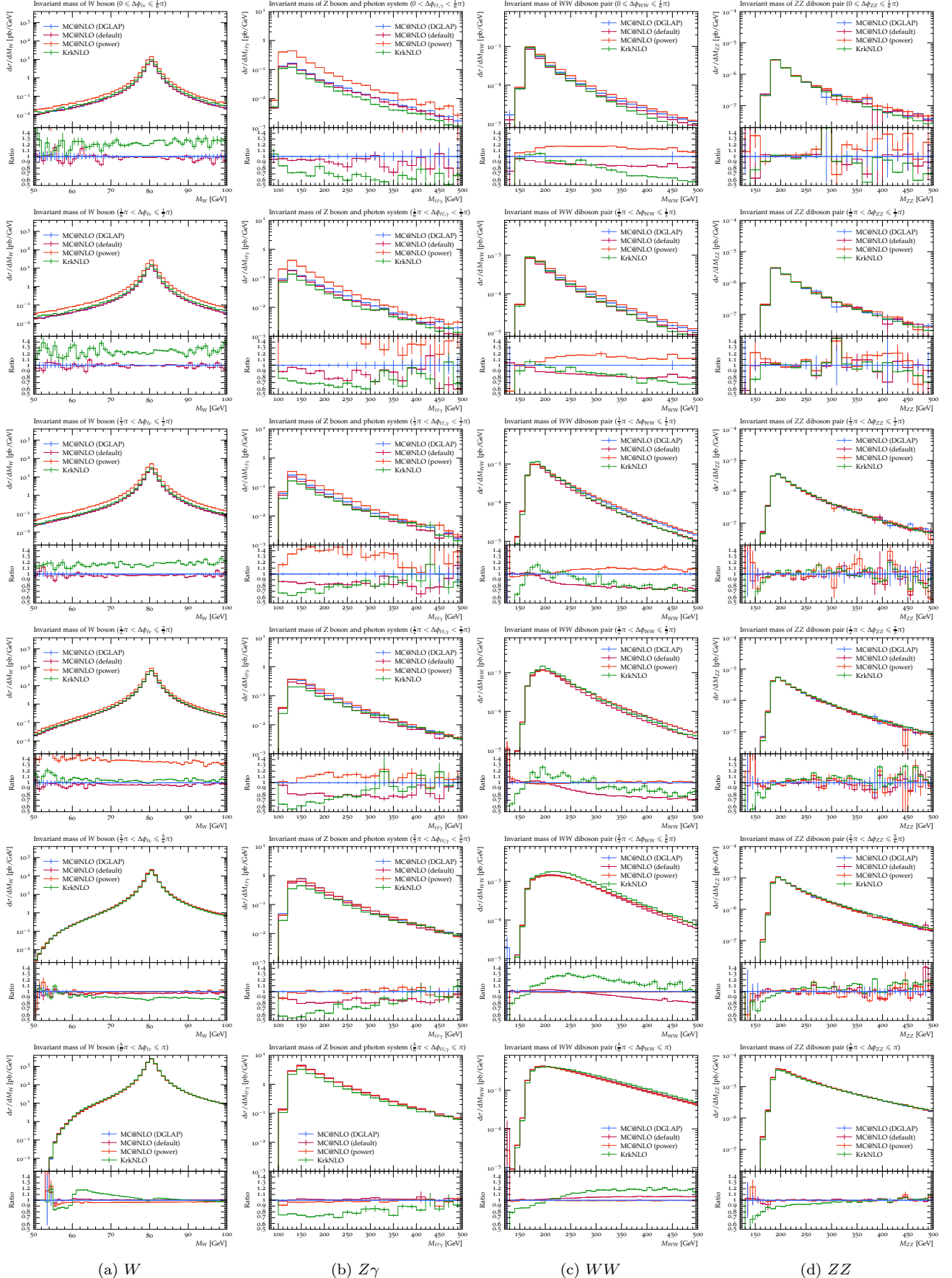


Figure 20: Full-shower comparison of the invariant mass of the colour-singlet system in slices of the azimuthal angle between the (reconstructed) two-particle constituents of the colour-singlet system; the complete partition of which a subset is shown in fig. 8.

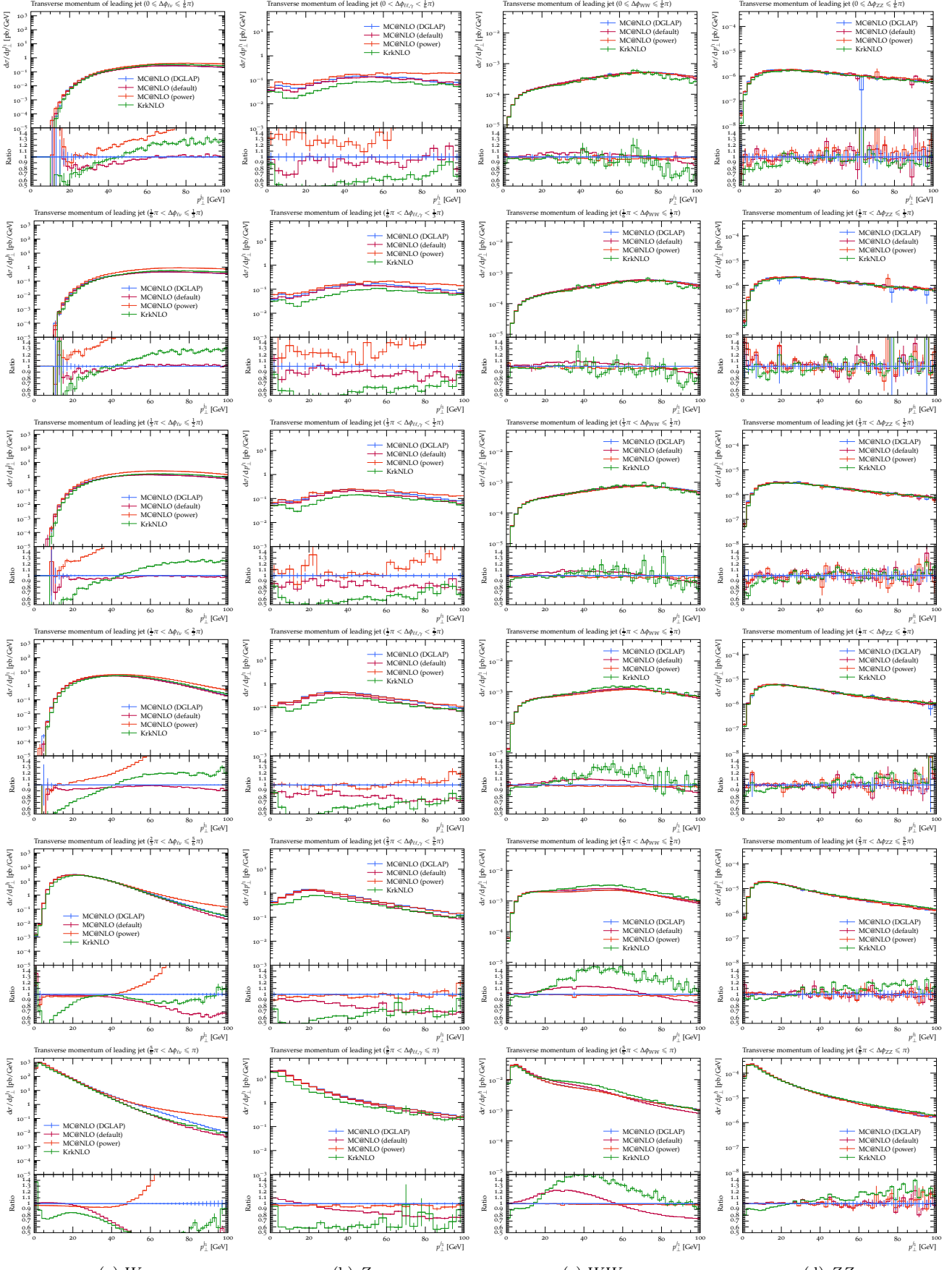


Figure 21: Full-shower comparison of the transverse momentum of the leading jet in slices of the azimuthal angle between the (reconstructed) two-particle constituents of the colour-singlet system; the complete partition of which a subset is shown in fig. 9.

References

- [1] S. Frixione and B.R. Webber, *Matching NLO QCD computations and parton shower simulations*, *JHEP* **06** (2002) 029 [[hep-ph/0204244](#)].
- [2] P. Nason, *A New method for combining NLO QCD with shower Monte Carlo algorithms*, *JHEP* **11** (2004) 040 [[hep-ph/0409146](#)].
- [3] S. Frixione, P. Nason and C. Oleari, *Matching NLO QCD computations with Parton Shower simulations: the POWHEG method*, *JHEP* **11** (2007) 070 [[0709.2092](#)].
- [4] S. Alioli, P. Nason, C. Oleari and E. Re, *A general framework for implementing NLO calculations in shower Monte Carlo programs: the POWHEG BOX*, *JHEP* **06** (2010) 043 [[1002.2581](#)].
- [5] W.T. Giele, D.A. Kosower and P.Z. Skands, *A simple shower and matching algorithm*, *Phys. Rev. D* **78** (2008) 014026 [[0707.3652](#)].
- [6] P. Nason and G.P. Salam, *Multiplicative-accumulative matching of NLO calculations with parton showers*, *JHEP* **01** (2022) 067 [[2111.03553](#)].
- [7] M. van Beekveld, S. Ferrario Ravasio, J. Helliwell, A. Karlberg, G.P. Salam, L. Scyboz et al., *Logarithmically-accurate and positive-definite NLO shower matching*, *JHEP* **10** (2025) 038 [[2504.05377](#)].
- [8] K. Hamilton, P. Nason and G. Zanderighi, *MINLO: Multi-Scale Improved NLO*, *JHEP* **10** (2012) 155 [[1206.3572](#)].
- [9] S. Alioli, C.W. Bauer, C.J. Berggren, A. Hornig, F.J. Tackmann, C.K. Vermilion et al., *Combining Higher-Order Resummation with Multiple NLO Calculations and Parton Showers in GENEVA*, *JHEP* **09** (2013) 120 [[1211.7049](#)].
- [10] S. Höche, Y. Li and S. Prestel, *Drell-Yan lepton pair production at NNLO QCD with parton showers*, *Phys. Rev. D* **91** (2015) 074015 [[1405.3607](#)].
- [11] P.F. Monni, P. Nason, E. Re, M. Wiesemann and G. Zanderighi, *MiNNLO_{PS}: a new method to match NNLO QCD to parton showers*, *JHEP* **05** (2020) 143 [[1908.06987](#)].
- [12] J.M. Campbell, S. Höche, H.T. Li, C.T. Preuss and P. Skands, *Towards NNLO+PS matching with sector showers*, *Phys. Lett. B* **836** (2023) 137614 [[2108.07133](#)].
- [13] S. Prestel, *Matching N3LO QCD calculations to parton showers*, *JHEP* **11** (2021) 041 [[2106.03206](#)].
- [14] S. Alioli, P. Nason, C. Oleari and E. Re, *NLO vector-boson production matched with shower in POWHEG*, *JHEP* **07** (2008) 060 [[0805.4802](#)].
- [15] S. Alioli, P. Nason, C. Oleari and E. Re, *NLO Higgs boson production via gluon fusion matched with shower in POWHEG*, *JHEP* **04** (2009) 002 [[0812.0578](#)].
- [16] S. Alioli, P. Nason, C. Oleari and E. Re, *NLO single-top production matched with shower in POWHEG: s- and t-channel contributions*, *JHEP* **09** (2009) 111 [[0907.4076](#)].
- [17] K. Hamilton, *A positive-weight next-to-leading order simulation of weak boson pair production*, *JHEP* **01** (2011) 009 [[1009.5391](#)].
- [18] S. Plätzer and S. Gieseke, *Dipole Showers and Automated NLO Matching in Herwig++*, *Eur. Phys. J. C* **72** (2012) 2187 [[1109.6256](#)].
- [19] S. Höche, F. Krauss, M. Schönherr and F. Siegert, *A critical appraisal of NLO+PS matching methods*, *JHEP* **09** (2012) 049 [[1111.1220](#)].
- [20] P. Nason and B. Webber, *Next-to-Leading-Order Event Generators*, *Ann. Rev. Nucl. Part. Sci.* **62** (2012) 187 [[1202.1251](#)].
- [21] R. Frederix, E. Re and P. Torrielli, *Single-top t-channel hadroproduction in the four-flavour scheme with POWHEG and aMC@NLO*, *JHEP* **09** (2012) 130 [[1207.5391](#)].
- [22] G. Heinrich, S.P. Jones, M. Kerner, G. Luisoni and E. Vryonidou, *NLO predictions for Higgs boson pair production with full top quark mass dependence matched to parton showers*, *JHEP* **08** (2017) 088 [[1703.09252](#)].

[23] S. Jones and S. Kuttmalai, *Parton Shower and NLO-Matching uncertainties in Higgs Boson Pair Production*, *JHEP* **02** (2018) 176 [[1711.03319](#)].

[24] K. Cormier, S. Plätzer, C. Reuschle, P. Richardson and S. Webster, *Parton showers and matching uncertainties in top quark pair production with Herwig 7*, *Eur. Phys. J. C* **79** (2019) 915 [[1810.06493](#)].

[25] B. Jäger, A. Karlberg, S. Plätzer, J. Scheller and M. Zaro, *Parton-shower effects in Higgs production via Vector-Boson Fusion*, *Eur. Phys. J. C* **80** (2020) 756 [[2003.12435](#)].

[26] ATLAS collaboration, *Studies on the improvement of the matching uncertainty definition in top-quark processes simulated with Powheg+Pythia 8*, Tech. Rep. [ATL-PHYS-PUB-2023-029](#), CERN, Geneva (2023).

[27] P. Sarmah, A. Siódtek and J. Whitehead, *KrkNLO matching for colour-singlet processes*, *JHEP* **01** (2025) 062 [[2409.16417](#)].

[28] S. Jadach, A. Kusina, W. Płaczek, M. Skrzypek and M. Ślawinska, *Inclusion of the QCD next-to-leading order corrections in the quark-gluon Monte Carlo shower*, *Phys. Rev. D* **87** (2013) 034029 [[1103.5015](#)].

[29] S. Jadach, W. Płaczek, S. Sapeta, A. Siódtek and M. Skrzypek, *Matching NLO QCD with parton shower in Monte Carlo scheme — the KrkNLO method*, *JHEP* **10** (2015) 052 [[1503.06849](#)].

[30] S. Jadach, G. Nail, W. Płaczek, S. Sapeta, A. Siódtek and M. Skrzypek, *Monte Carlo simulations of Higgs-boson production at the LHC with the KrkNLO method*, *Eur. Phys. J. C* **77** (2017) 164 [[1607.06799](#)].

[31] J. Bellm et al., *Herwig 7.0/Herwig++ 3.0 release note*, *Eur. Phys. J. C* **76** (2016) 196 [[1512.01178](#)].

[32] G. Bewick et al., *Herwig 7.3 release note*, *Eur. Phys. J. C* **84** (2024) 1053 [[2312.05175](#)].

[33] S. Jadach, W. Płaczek, S. Sapeta, A. Siódtek and M. Skrzypek, *Parton distribution functions in Monte Carlo factorisation scheme*, *Eur. Phys. J. C* **76** (2016) 649 [[1606.00355](#)].

[34] F. Buccioni, J.-N. Lang, J.M. Lindert, P. Maierhöfer, S. Pozzorini, H. Zhang et al., *OpenLoops 2*, *Eur. Phys. J. C* **79** (2019) 866 [[1907.13071](#)].

[35] S. Delorme, A. Kusina, A. Siódtek and J. Whitehead, *Factorisation schemes for proton PDFs*, *Eur. Phys. J. C* **85** (2025) 505 [[2501.18289](#)].

[36] C. Bierlich et al., *Robust Independent Validation of Experiment and Theory: Rivet version 3*, *SciPost Phys.* **8** (2020) 026 [[1912.05451](#)].

[37] PARTICLE DATA GROUP collaboration, *Review of Particle Physics*, *PTEP* **2022** (2022) 083C01.

[38] S. Plätzer and S. Gieseke, *Coherent Parton Showers with Local Recoils*, *JHEP* **01** (2011) 024 [[0909.5593](#)].

[39] Z. Nagy and D.E. Soper, *Matching parton showers to NLO computations*, *JHEP* **10** (2005) 024 [[hep-ph/0503053](#)].

[40] Z. Nagy and D.E. Soper, *A new parton shower algorithm: Shower evolution, matching at leading and next-to-leading order level*, in *Ringberg Workshop on New Trends in HERA Physics 2005*, pp. 101–123, 1, 2006, DOI [[hep-ph/0601021](#)].

[41] M. Dinsdale, M. Ternick and S. Weinzierl, *Parton showers from the dipole formalism*, *Phys. Rev. D* **76** (2007) 094003 [[0709.1026](#)].

[42] S. Schumann and F. Krauss, *A parton shower algorithm based on Catani-Seymour dipole factorisation*, *JHEP* **03** (2008) 038 [[0709.1027](#)].

[43] S. Catani and M.H. Seymour, *A General algorithm for calculating jet cross-sections in NLO QCD*, *Nucl. Phys. B* **485** (1997) 291 [[hep-ph/9605323](#)].

[44] J. Bellm, G. Nail, S. Plätzer, P. Schichtel and A. Siódtek, *Parton Shower Uncertainties with Herwig 7: Benchmarks at Leading Order*, *Eur. Phys. J. C* **76** (2016) 665 [[1605.01338](#)].

[45] T.-J. Hou et al., *New CTEQ global analysis of quantum chromodynamics with high-precision data from the LHC*, *Phys. Rev. D* **103** (2021) 014013 [[1912.10053](#)].

[46] S. Frixione, *Isolated photons in perturbative QCD*, *Phys. Lett. B* **429** (1998) 369 [[hep-ph/9801442](#)].

[47] J.R. Andersen et al., *Les Houches 2013: Physics at TeV Colliders: Standard Model Working Group Report*, [1405.1067](#).

[48] M. Cacciari, G.P. Salam and G. Soyez, *The anti- k_t jet clustering algorithm*, *JHEP* **04** (2008) 063 [[0802.1189](#)].

[49] C. Duhr, F. Dulat and B. Mistlberger, *Charged current Drell-Yan production at N^3LO* , *JHEP* **11** (2020) 143 [[2007.13313](#)].

[50] X. Chen, T. Gehrmann, E.W.N. Glover, A. Huss, P.F. Monni, E. Re et al., *Third-Order Fiducial Predictions for Drell-Yan Production at the LHC*, *Phys. Rev. Lett.* **128** (2022) 252001 [[2203.01565](#)].

[51] X. Chen, T. Gehrmann, E.W.N. Glover, A. Huss, T.-Z. Yang and H.X. Zhu, *Transverse mass distribution and charge asymmetry in W boson production to third order in QCD*, *Phys. Lett. B* **840** (2023) 137876 [[2205.11426](#)].

[52] J. Campbell and T. Neumann, *Third order QCD predictions for fiducial W -boson production*, *JHEP* **11** (2023) 127 [[2308.15382](#)].

[53] A. Karlberg, E. Re and G. Zanderighi, *NNLOPS accurate Drell-Yan production*, *JHEP* **09** (2014) 134 [[1407.2940](#)].

[54] S. Alioli, C.W. Bauer, C. Berggren, F.J. Tackmann and J.R. Walsh, *Drell-Yan production at NNLL'+NNLO matched to parton showers*, *Phys. Rev. D* **92** (2015) 094020 [[1508.01475](#)].

[55] R. Boughezal, C. Focke, X. Liu and F. Petriello, *W -boson production in association with a jet at next-to-next-to-leading order in perturbative QCD*, *Phys. Rev. Lett.* **115** (2015) 062002 [[1504.02131](#)].

[56] R. Boughezal, X. Liu and F. Petriello, *W -boson plus jet differential distributions at NNLO in QCD*, *Phys. Rev. D* **94** (2016) 113009 [[1602.06965](#)].

[57] A. Gehrmann-De Ridder, T. Gehrmann, E.W.N. Glover, A. Huss and D.M. Walker, *Next-to-Next-to-Leading-Order QCD Corrections to the Transverse Momentum Distribution of Weak Gauge Bosons*, *Phys. Rev. Lett.* **120** (2018) 122001 [[1712.07543](#)].

[58] NNLOJET collaboration, *NNLOJET: a parton-level event generator for jet cross sections at NNLO QCD accuracy*, [2503.22804](#).

[59] ATLAS collaboration, *Measurement of the inclusive W^\pm and Z/γ^* cross sections in the electron and muon decay channels in pp collisions at $\sqrt{s} = 7$ TeV with the ATLAS detector*, *Phys. Rev. D* **85** (2012) 072004 [[1109.5141](#)].

[60] ATLAS collaboration, *Measurements of the W production cross sections in association with jets with the ATLAS detector*, *Eur. Phys. J. C* **75** (2015) 82 [[1409.8639](#)].

[61] M. Grazzini, S. Kallweit, D. Rathlev and A. Torre, *$Z\gamma$ production at hadron colliders in NNLO QCD*, *Phys. Lett. B* **731** (2014) 204 [[1309.7000](#)].

[62] M. Grazzini, S. Kallweit and D. Rathlev, *$W\gamma$ and $Z\gamma$ production at the LHC in NNLO QCD*, *JHEP* **07** (2015) 085 [[1504.01330](#)].

[63] J.M. Campbell, T. Neumann and C. Williams, *$Z\gamma$ Production at NNLO Including Anomalous Couplings*, *JHEP* **11** (2017) 150 [[1708.02925](#)].

[64] D. Lombardi, M. Wiesemann and G. Zanderighi, *Advancing MiNNLOPS to diboson processes: $Z\gamma$ production at NNLO+PS*, *JHEP* **06** (2021) 095 [[2010.10478](#)].

[65] A. Denner, S. Dittmaier, M. Hecht and C. Pasold, *NLO QCD and electroweak corrections to $Z + \gamma$ production with leptonic Z -boson decays*, *JHEP* **02** (2016) 057 [[1510.08742](#)].

[66] ATLAS collaboration, *Measurement of the $Z(\rightarrow \ell^+ \ell^-)\gamma$ production cross-section in pp collisions at $\sqrt{s} = 13$ TeV with the ATLAS detector*, *JHEP* **03** (2020) 054 [[1911.04813](#)].

[67] T. Gehrmann, M. Grazzini, S. Kallweit, P. Maierhöfer, A. von Manteuffel, S. Pozzorini et al., *W^+W^- Production at Hadron Colliders in Next to Next to Leading Order QCD*, *Phys. Rev. Lett.* **113** (2014) 212001 [[1408.5243](#)].

[68] M. Grazzini, S. Kallweit, S. Pozzorini, D. Rathlev and M. Wiesemann, *W^+W^- production at the LHC: fiducial cross sections and distributions in NNLO QCD*, *JHEP* **08** (2016) 140 [[1605.02716](#)].

[69] R. Poncelet and A. Popescu, *NNLO QCD study of polarised W^+W^- production at the LHC*, *JHEP* **07** (2021) 023 [[2102.13583](#)].

[70] E. Re, M. Wiesemann and G. Zanderighi, *NNLOPS accurate predictions for W^+W^- production*, *JHEP* **12** (2018) 121 [[1805.09857](#)].

[71] D. Lombardi, M. Wiesemann and G. Zanderighi, *W^+W^- production at NNLO+PS with MINNLO_{PS}*, *JHEP* **11** (2021) 230 [[2103.12077](#)].

[72] A. Gavardi, M.A. Lim, S. Alioli and F.J. Tackmann, *NNLO+PS W^+W^- production using jet veto resummation at NNLL'*, *JHEP* **12** (2023) 069 [[2308.11577](#)].

[73] M. Grazzini, S. Kallweit, J.M. Lindert, S. Pozzorini and M. Wiesemann, *NNLO QCD + NLO EW with Matrix+OpenLoops: precise predictions for vector-boson pair production*, *JHEP* **02** (2020) 087 [[1912.00068](#)].

[74] ATLAS collaboration, *Measurement of fiducial and differential W^+W^- production cross-sections at $\sqrt{s} = 13$ TeV with the ATLAS detector*, *Eur. Phys. J. C* **79** (2019) 884 [[1905.04242](#)].

[75] F. Cascioli, T. Gehrmann, M. Grazzini, S. Kallweit, P. Maierhöfer, A. von Manteuffel et al., *ZZ production at hadron colliders in NNLO QCD*, *Phys. Lett. B* **735** (2014) 311 [[1405.2219](#)].

[76] M. Grazzini, S. Kallweit and D. Rathlev, *ZZ production at the LHC: fiducial cross sections and distributions in NNLO QCD*, *Phys. Lett. B* **750** (2015) 407 [[1507.06257](#)].

[77] S. Kallweit and M. Wiesemann, *ZZ production at the LHC: NNLO predictions for $2\ell 2\nu$ and 4ℓ signatures*, *Phys. Lett. B* **786** (2018) 382 [[1806.05941](#)].

[78] G. Heinrich, S. Jahn, S.P. Jones, M. Kerner and J. Pires, *NNLO predictions for Z -boson pair production at the LHC*, *JHEP* **03** (2018) 142 [[1710.06294](#)].

[79] C. Carrivale et al., *Precise Standard-Model predictions for polarised Z -boson pair production and decay at the LHC*, [2505.09686](#).

[80] S. Alioli, A. Broggio, A. Gavardi, S. Kallweit, M.A. Lim, R. Nagar et al., *Next-to-next-to-leading order event generation for Z boson pair production matched to parton shower*, *Phys. Lett. B* **818** (2021) 136380 [[2103.01214](#)].

[81] L. Buonocore, G. Koole, D. Lombardi, L. Rottoli, M. Wiesemann and G. Zanderighi, *ZZ production at n NNLO+PS with MiNNLO_{PS}*, *JHEP* **01** (2022) 072 [[2108.05337](#)].

[82] B. Agarwal, S. Jones, M. Kerner and A. von Manteuffel, *Complete Next-to-Leading Order QCD Corrections to ZZ Production in Gluon Fusion*, *Phys. Rev. Lett.* **134** (2025) 031901 [[2404.05684](#)].

[83] ATLAS collaboration, *$ZZ \rightarrow \ell^+\ell^-\ell'^+\ell'^-$ cross-section measurements and search for anomalous triple gauge couplings in 13 TeV pp collisions with the ATLAS detector*, *Phys. Rev. D* **97** (2018) 032005 [[1709.07703](#)].

[84] J.C. Collins and D.E. Soper, *Parton Distribution and Decay Functions*, *Nucl. Phys. B* **194** (1982) 445.